Title: **Novel Pannexin 1 isoform is increased in cancer**

Authors: **Brooke L. O'Donnell[1], Dan Stefan[1], Yu-Hsin Chiu[2,3] Michael J. Zeitz[4], Justin Tang[1], Danielle Johnston[1], Stephanie E. Leighton[1], Carlijn Van Kessel[1], Kevin Barr[1], Laszlo Gyenis[5], Taylor J. Freeman[1], John J. Kelly[6,7], Samar Sayedyahossein[1,8], Brant E. Isakson[9], David W. Litchfield[5,10], Kathryn Roth[11,12], James W. Smyth[4,13,14], Matthew Hebb[9,15], John Ronald[6,7,10], Douglas A. Bayliss[2], Silvia Penuela[1,10*]**

Affiliations:

[1]Department of Anatomy and Cell Biology, Schulich School of Medicine and Dentistry, University of Western Ontario, London, Ontario, Canada, N6A 5C1.

[2]Department of Pharmacology, University of Virginia School of Medicine, Charlottesville, Virginia, USA, 22908.

[3]Institute of Biotechnology, National Tsing Hua University, Hsinchu, Taiwan, 300044.

[4]Fralin Biomedical Research Institute atVirginia Tech Carilion, Roanoke, Virginia, USA, 24016.

[5]Department of Biochemistry, Schulich School of Medicine and Dentistry, University of Western Ontario, London, Ontario, Canada, N6A 5C1.

[6]Department of Medical Biophysics, Schulich School of Medicine and Dentistry, University of Western Ontario, London, Ontario, Canada, N6A 5C1.

[7]Robarts Research Institute, University of Western Ontario, London, Ontario, Canada, N6A 3K7.

[8]Department of Laboratory Medicine, National Institutes of Health, Bethesda, Maryland, USA, 20892

[9]Department of Molecular Physiology and Biological Physics, University of Virginia School of Medicine, Charlottesville, Virginia, USA, 22908.

[10]Department of Oncology, Division of Experimental Oncology, Schulich School of Medicine and Dentistry, University of Western Ontario, London, Ontario, Canada, N6A 5C1.

[11]Department of Otolaryngology—Head and Neck Surgery, Schulich School of Medicine and Dentistry, University of Western Ontario, London, Ontario, Canada, N6A 5C1.

[12]London Regional Cancer Program, London Health Sciences Centre, London, Ontario, Canada, N6A 5W9.

[13]Virginia Tech Carilion School of Medicine, Roanoke, Virginia, USA, 24016.

[14]Department of Biological Sciences, College of Science, Virginia Polytechnic Institute and State University, Blacksburg, Virginia, USA, 24060.

[15]Department of Clinical Neurological Sciences, Schulich School of Medicine and Dentistry, University of Western Ontario, London, Ontario, Canada, N6A 3K7.

*Corresponding author: Silvia Penuela, Associate Professor, Department of Anatomy and Cell Biology, University of Western Ontario, London, Ontario, Canada. Tel. 519-661-2111 ext. 84735; E-mail: spenuela@uwo.ca

Running title: PANX1-25K in cancer

ABSTRACT

Pannexin 1 (PANX1) is upregulated in many cancers, where its channel activity and signalling promote tumorigenic properties. Here, we report that potential internal translation start sites exist in mouse and human PANX1 which have implications in trafficking and protein interaction. Using mouse PANX1 constructs for each internal methionine (M) we saw that the shorter PANX1 isoforms were glycosylated, able to traffic to the cell surface and PANX1-M37 formed channels which could be activated by C-terminus cleavage or α1-adrenoceptor stimulation. Furthermore, we report a novel ~25 kDa isoform of human PANX1 (hPANX1-25K) which lacks the N-terminus and was detected in several human cancer cell lines including melanoma, osteosarcoma, breast cancer, and glioblastoma multiforme. This isoform was increased upon *hPANX1* CRISPR/Cas9 deletion targeting the first exon near M1, and using Expasy PeptideCutter we did not find any evidence of hPANX1 cleavage sites which would produce a 25 kDa fragment, suggesting a potential alternative translation initiation site as the source of hPANX1-25K. hPANX1-25K was confirmed to be a hPANX1 isoform via mass spectrometry, can be N-linked glycosylated at multiple sites including the canonical N255 and novel N338 and N394 residues, and can interact with both β-catenin and full length hPANX1. Using cell surface biotinylation and immunocytochemistry, we also determined hPANX1-25K exhibits a predominantly intracellular localization. hPANX1-25K is prevalent throughout melanoma progression, and its levels are increased in squamous cell carcinoma cells and patient-derived tumours, compared to keratinocytes and patient-matched normal skin, indicating that it may be differentially regulated in normal and cancer cells.

KEYWORDS

PANX1, PANX1-25K, isoform, alternative translation initiation, cancer, mouse, human

INTRODUCTION

Pannexins (PANX1, PANX2, PANX3) are heptameric, channel-forming glycoproteins which have been associated with the initiation and progression of various cancers[1-3]. PANX1 specifically has

been implicated in many cancer types, and is generally present at high levels in colon[4], leukemia[5], melanoma[6-8], cutaneous squamous cell carcinoma (cSCC)[9], glioma[10], breast[11-13], prostate[14], and testicular[15] tumours. High PANX1 levels are associated with poor prognosis in renal, lung, and endometrial cancers[1], as well as poor survival in breast cancer patients[13]. Adenocarcinoma of the gall bladder[16], rhabdomyosarcoma[17], and basal cell carcinoma[7] are exceptions, in that PANX1 exhibits a lower abundance compared to normal tissue. PANX1 upregulation in cancers such as melanoma[6,8], breast cancer[11,12], and glioblastoma multiforme (GBM)[10] promotes tumorigenic and metastatic properties where hyperactive PANX1 channels facilitate processes involved in tumorigenesis such as growth, migration, invasion, and epithelial-mesenchymal transition (EMT)[6,12,15]. Channel-independent, pro-tumorigenic functions for pannexins have also emerged more recently. We have shown that PANX1 directly binds to the Wnt pathway effector β-catenin (CTNNB1) in melanoma cells, where PANX1-mediated stabilization of β-catenin regulates melanoma cell growth and mitochondrial respiratory activity[8]. In highly metastatic breast cancer cells, a shorter version of hPANX1 resulting from a nonsense mutation and containing only the first 89 amino acids ($PANX1^{1-89}$) was identified. Through augmented ATP release and downstream purinergic signalling, the $PANX1^{1-89}$ mutant promotes the survival of metastatic cells during the process of extravasation at a secondary microvasculature site, where cells would otherwise die from intravascular deformation of the plasma membrane[11].

In addition to $PANX1^{1-89}$, other pannexin isoform transcripts generated through alternative splicing or truncations have been identified in rodents and humans, but few have been detected at the protein level[18]. RefSeq *PANX1*[19] (also annotated as PANX1b[20] and PANX1-201 in Ensembl[21]) contains 5 exons and 4 introns that can be alternatively spliced at exon 2, 4[22] and 5[23] to produce PANX1c, PANX1d and PANX1a transcript isoforms, respectively. Another PANX1 splice variant which lacks exon 3 was detected in the reproductive tract of male rats, where its abundance may be regulated by androgens[24]. The PANX2-202 splice variant was detected in mouse dorsal skin[25] where it is present at higher levels than the canonical full length PANX2 and is temporally regulated during skin aging[26]. Lastly, a translationally incompetent *PANX1* transcript variant which lacks the 5' untranslated region was identified in rhabdomyosarcoma cells, resulting in a reduction in PANX1 levels in rhabdomyosarcoma cells compared to normal skeletal muscle myoblasts despite containing similar amounts of *PANX1* mRNA[27]. Thus, because the pannexin family only contains three genes, alternative splicing is one way to increase pannexin protein

diversity in different cell types and these pannexin isoforms may have distinct cellular consequences such as altered channel activity and signalling. However, the presence of pannexin proteoforms in cancer is yet to be investigated.

Another way to increase the coding capacity of genes is through the process of alternative translation initiation (ATI) which is exploited by cancer cells to cope with cellular stresses common in the cancer microenvironment that often inhibit canonical, cap-dependent translation[28]. For example, connexin 43 (Cx43, *GJA1*), a member of the connexin and pannexin protein families, was shown to produce ATI variants in cancerous and non-cancerous cells, where truncated isoforms such as GJA1-20k autoregulate Cx43 hexamer oligomerization, trafficking, and gap junction formation [29,30 31,32] Interestingly, GJA1-20k had cardioprotective effects in disease states such as chronic ischemia and ischemia reperfusion injury when overexpressed[33,34] but was downregulated in aged hearts, hypoxic and TGF-β-treated cells, and in human arrhythmogenic cardiomyopathy [35-37]. Furthermore, GJA1-20k is downregulated during EMT, a process that promotes cancer progression, during which cells must remodel cell-cell adhesions and junctions to facilitate migration [31,38]. Overall, this indicates GJA1-20k levels are dynamically regulated to control gap junction formation in normal physiology as well as pathologically during aging, disease, or cellular stress. However, whether PANX1 undergoes ATI is currently unknown.

In this study, we analyzed mouse PANX1 (mPANX1) and human PANX1 (hPANX1) to identify novel variants of this channel forming protein and investigated their relevance in a cancer context. When examining the PANX1 protein sequence, we observed multiple internal methionine (Met, M) residues and one isoleucine residue (Ile, I; I211 in humans, M210 in mice) which could function as potential ATI sites[39]. Looking at endogenous protein expression, we discovered a ~25 kDa immunoreactive species (hPANX1-25K) in many human cancer cell lines corresponding to the predicted size of the I211 ATI site which we positively identified as an isoform of hPANX1 through mass spectrometry. hPANX1-25K is predicted to contain part of the intracellular loop, second extracellular loop and the complete C-terminus (CT). This novel variant increases upon *hPANX1* CRISPR/Cas9 deletion targeting the canonical hPANX1 start site (M1). Transcriptomic analysis suggested hPANX1-25K does not originate from alternative transcription or splicing, and thus, we propose hPANX1-25K may originate from ATI of the full length *hPANX1* transcript. hPANX1-25K exhibits an intracellular localization, can be N-linked glycosylated and interacts with full length hPANX1 and β-catenin. Lastly, hPANX1-25K levels were increased in cSCC

compared to non-transformed skin and/or keratinocyte cell lines, suggesting that hPANX1-25K may exert pro-tumorigenic functions.

RESULTS

Multiple ATI sites are present in mPANX1 and their products localize to the plasma membrane, but only M37 forms functional channels which require activation

By analyzing the mouse *mPANX1* transcript sequence, we found 4 additional in-frame AUG codons downstream of the canonical start site at M1, including M37, M143, M210 and M374 **(Figure 1A)**. Consistent with the possibility of multiple ATI sites, we observed a range of HA-immunoreactive bands (from ~30-60 kDa) in HEK293T cells expressing mPANX1 with a CT HA tag (mPANX1-HA) via western blotting **(Figure 1B)**. While complex N-glycosylation at N254 of mPANX1 could lead to multiple immunoreactive bands[40,41], the deglycosylated samples treated by Peptide-*N*-Glycosidase F (PNGase F) showed a similar, but shifted banding pattern (now ranging from ~25-50 kDa), indicating that the different sizes were not due to differential glycosylation. In congruence with the possibility of multiple in-frame isoforms, each internal Met is surrounded with the Kozak initiation consensus sequence (RxxAUGG; R=A/G) crucial for translation initiation[42] **(Figure 1C)**. To examine whether the identified AUG codons could function as potential start sites, we generated a series of mutant mPANX1 constructs where we retained only one Met codon and included Ile substitutions at all other sites to markedly reduce translation efficiency. We found a single immunoreactive band in blots from HEK293T cells expressing HA-tagged mPANX1 constructs that retained only a single ATI site. The apparent molecular weights of these HA antibody-detected signals were consistent with those estimated from the predicted ATI sites, further verifying that M37, M143, M210 can serve as translation initiation sites alternative to the conventional M1. Notably, no protein expression of the M374-only form of mPANX1 was detectable in HEK293T cells following transient transfections **(Figure 1D)**.

To determine whether the alternatively translated mPANX1 proteins trafficked to the plasma membrane, we performed cell surface biotinylation assays and found a similar level of cell surface expression for mPANX1 translated using M1-only as compared with wildtype (WT) mPANX1 **(Figure 2A)**. While the other mPANX1 variants could also be detected at the cell surface (M37-

only, M143-only, and M210-only), the levels of the alternatively translated mPANX1 forms were relatively lower than the WT or M1-only constructs in total cell lysates and at the cell surface **(Figure 2A)**. To determine whether different mPANX1 ATI forms act as a functional ion channel at the plasma membrane, we performed whole-cell voltage clamp recordings in HEK293T cells expressing the mutant forms of mPANX1 **(Figure 2B)**. We found that, similar to the WT mPANX1[43], the M1-only form of mPANX1 was basally active in HEK293T cells, as evidenced by the presence of carbenoxolone (CBX)-sensitive, outwardly-rectifying currents. While both M1 and M37 translational initiation sites can produce a polypeptide with four intact transmembrane domains and are presumably capable of forming a complete mPANX1 channel complex, to our surprise, we did not observe any basal currents after expressing the M37-only form of mPANX1 in HEK293T cells. Similarly, the M143-only and M210-only mPANX1 forms did not display any channel activity. Notably, the whole-cell current of the M1-only form of mPANX1 displayed a more striking outwardly rectifying current-voltage (I-V) relationship than WT mPANX1, with no observable CBX-sensitive current at negative membrane potentials **(Figure 2C)**. The mechanism for the altered I-V relationship remains unclear but is likely due to mutational effects of the downstream methionine substitutions.

To determine whether mPANX1 M37-only is capable of forming functional channels that require activation such as through the removal of the CT tail previously demonstrated for WT mPANX1[43,44], we generated an M37-only (Tobacco Etch Virus, TEV) construct by replacing the CT caspase 3/7 cleavage site of mPANX1 M37-only with the TEV protease (TEVp) recognition sequence[43]. Co-expression of M37-only (TEV) together with TEVp in HEK293T cells resulted in CBX-sensitive currents that were absent in cells co-expressing M37-only (TEV) and red fluorescence protein (RFP) or the M37-only construct with TEVp **(Figure 2D)**. This indicates that mPANX1 M37-only can constitute functional cleavage-activated channels that are basally silent. To determine whether this form of mPANX1 can also be activated by receptor signaling pathways[45], we co-expressed M37-only and the mouse α1D adrenoceptor in HEK293T cells and found that bath application of the α1 adrenoceptor agonist phenylephrine (PE) induced a CBX-sensitive PANX1 current that was not observed in cells expressing mPANX1 M37-only alone **(Figure 2E)**. This further verifies that mPANX1 M37-only can form functional channels that require activation by multiple mechanisms. Unlike the strongly outwardly rectifying I-V relationship observed in cells expressing mPANX1 M1-only **(Figure 2B inset)**, the I-V

relationships observed from the TEVp-activated M37-only(TEV) channels **(Figure 2D, left panel)** and α1D adrenoceptor-activated M37-only channels **(Figure 2E, right panel)** were similar to those observed from mPANX1 WT[43,45].

hPANX1 also contains possible ATI sites

Like with mPANX1, we discovered additional amino acid residues throughout hPANX1 which could function as possible sites of internal translation **(Figure 3A, B)**, including nine internal Met residues and one Ile residue (I211, corresponding to M210 in mice). All start sites are retained in the intracellular domains of hPANX1, with one in the N-terminus (NT), three in the intracellular loop and six in the CT, with predicted molecular weights ranging from 2.8 kDa to 44 kDa. The M37, M143, M165 and I211 potential isoforms retain multiple transmembrane domains, indicating they could be integral membrane proteins—as well as many hPANX1 post-translational modification sites. Analysis of the canonical *hPANX1* transcript for the Kozak initiation sequence at each potential internal start site **(Figure 3C)** revealed moderate to high sequence similarity to the consensus sequence at most sites. Interestingly, I211 shows evolutionary conservation in most primate species, whereas rodents have either a methionine or valine (Val, V) at the corresponding amino acid position 210 **(Figure S1)**. Codons encoding both Ile and Val have been previously shown to act as non-canonical ATI start sites[39]. Additionally, exogenous expression of wildtype hPANX1 (hPANX1 WT) in Hs578T *hPANX1* knockout (KO) cells presented four immunoreactive species detectable by the PANX1 CT-412 antibody (targeting the end of the CT including residues 412-426[41]) which appeared to have lower molecular weights than the canonical full length hPANX1 bands **(Figure 3D)**, resembling some of those observed with mPANX1-HA **(Figure 1B)**.

The hPANX1-25K isoform is present in several cell types and increases upon ablation of the first methionine (M1)

When we surveyed various human patient-derived and established cell lines to identify endogenous isoforms of hPANX1, we discovered a prominent ~25 kDa immunoreactive species (hPANX1-25K) in western blots of human osteosarcoma, melanoma, breast cancer, and GBM cells which roughly corresponded to the 24.3 kDa predicted molecular weight of the I211 internal start site variant and can sometimes appear as a doublet **(Figure 4A, B)**. In human keratinocyte (N/TERT-1) and cSCC (SCC-13) cell lines, we found that hPANX1-25K levels and the ratio of

hPANX1-25K to full length hPANX1 were significantly higher in SCC-13 cells compared to N/TERT-1 cells, indicating this shorter immunoreactive species is present in multiple tissue types but may be upregulated in cancer cells **(Figure 4C)**. However, the elevated levels of this 25K species were not due to an I211M mutation present in SCC-13 cancer cells since genomic sequencing of SCC-13 cells, as well as other cancerous and non-cancerous cell lines used in this study, identified an 'ATC' in the genomic DNA sequence of *hPANX1* corresponding to the 211th amino acid in the hPANX1 peptide sequence **(Figure 4D)**. The 'ATC' nucleotide sequence encodes for Ile and is consistent with what is reported in NCBI RefSeq[19]. Structurally, a variant derived from the Ile-211 initiation site is predicted to contain transmembrane domains 3 and 4, the second extracellular loop and the CT tail of full length hPANX1 suggesting that it may integrate into cell and/or organelle membranes. Additionally, the protein would retain the glycosylation site at N254[41], phosphorylation site at Y309[46,47] and caspase cleavage site at D376-D379[43,44] of the full-length protein **(Figure 4E)**.

The 25K immunoreactive species was detected when blots were probed with the PANX1 CT-412 antibody. Upon full length *hPANX1* CRISPR/Cas9 deletion in HEK, Hs578T and GBM17 cells, where guide RNA (gRNA) targeted the canonical M1 start site at the beginning of exon 1 (KO), the levels of the 25K variant were found to be significantly increased in each cell type compared to WT controls and negatively correlated with hPANX1 levels **(Figure 5A-F)**. However, the 25K band was not seen when blots were probed with NT PANX1 antibodies **(Figure 5G-I)**, confirming that the 25K variant does not include the NT of hPANX1. Interestingly, despite the deletion of full length *hPANX1* in HEK, Hs578T, and GBM17 cells, RT-qPCR using primers targeting the middle region of the canonical *hPANX1* mRNA showed *hPANX1* transcript levels were similar between WT and *hPANX1* KO cells **(Figure 5J-L)**. Transcriptomic analysis using Cap Analysis of Gene Expression sequencing (CAGE-seq) data from the FANTOM 5 project[48-50] and Nanopore long read RNA sequencing mined from a previous study[51] suggested that hPANX1-25K does not originate from an alternative transcription initiation site, alternative promoter usage, or alternative transcript splicing of *mPANX1* or *hPANX1* **(Figure S2)**. However, we cannot rule out a transcript isoform without deeper RNA sequencing analysis from the cell lines used in this study. Furthermore, analysis of full length hPANX1 within 10 residues of the I211 position for cleavage sites using Expasy PeptideCutter[52] **(Figure S3A)** and pro-peptide cleavage sites using ProP 1.0 software[53] **(Figure S3B)** did not show evidence of any biologically relevant or naturally

occurring cleavage sites, nor pro-peptide cleavage sites which would produce a 25 kDa peptide fragment.

hPANX1-25K is an isoform of hPANX1

To positively identify the 25K immunoreactive band as an isoform of hPANX1, we immunoprecipitated hPANX1 proteins from the aggressive melanoma cell line 131/4-5B1, using the PANX1 CT-412 antibody and analyzed individual band samples excised from a GelCode Blue stained gel by liquid chromatography–mass spectrometry/mass spectrometry (LC-MS/MS) (**Figure 6A**). MS analyses of the 25K band detected the presence of multiple peptide fragments corresponding to the CT of hPANX1 (**Figure 6B**), unlike those of full length hPANX1 which identified peptide fragments mapping to all domains of the protein, including the NT (**Figure S4)**. These results strongly support our hypothesis that the 25K immunoreactive band represents a novel variant of hPANX1 (hereafter called hPANX1-25K) that does not include the NT of hPANX1.

Assuming hPANX1-25K begins at the I211 predicted start site, we performed topology predictions for hPANX1 residues I211-C426 using ΔG prediction server v1.0 (**Figure S5A**), TOPCONS (**Figure S5B**), Dense Alignment Surface (**Figure S5C**), and SOSUI (**Figure S5D**) software. Each of these platforms predicted that the topology matches the canonical hPANX1 topology starting at residue I211 (with cytoplasmic NT and CT domains, two transmembrane domains and one extracellular loop) except including a potential membrane interacting region corresponding to the hPANX1 sequence flanking residue L370 (**Figure S5E**). DeepTMHMM (**Figure S5F**) software predicted the canonical topology for hPANX1 I211-C426 (**Figure 4E**). Surprisingly, further topological predictions using MemPype (**Figure S6A**) software indicated a different topology in which the NT is cytoplasmic, followed by one transmembrane domain and an extracellular facing CT (**Figure S6B**). hPANX1 I211-C426 had a high internal membrane score of 88% and low cell membrane (-23%), as opposed to full length hPANX1 which scored highly for both cell membrane and internal membranes at 73% and 89% (**Figure S6A**). A signal peptide region of unknown significance was also predicted at the NT of the I211-C426 sequence, corresponding to hPANX1 residues I211 to K267 which was not seen with the same analysis of the full-length protein (**Figure S6A**).

hPANX1-25K exhibits intracellular localization and interacts with hPANX1

Next, we designed hPANX1 mutant plasmids to investigate hPANX1-25K trafficking, including constructs that contain only the hPANX1 sequence starting from M143, M165 or the predicted hPANX1-25K alternative start site (I211). We also generated a construct containing the hPANX1 sequence starting at amino acid 211, but with a Met instead of an Ile start (M211) to force translation in an ectopic expression setting. WT, M143, M165, I211, and M211 constructs were expressed alone or M211 was co-expressed with WT in Hs578T *hPANX1* KO cells. While M143 (top species 32.9 kDa, lower species 30.3 kDa) and M165 (top species 30.91 kDa, lower species 28.02 kDa) were higher in molecular weight than endogenous hPANX1-25K (**Figure S7A**), we found that M211 expression resulted in a banding pattern corresponding to hPANX1-25K (taking into consideration that the HA tag adds approximately 1 kDa to the molecular weight) with a doublet containing 26.0 kDa and 22.4 kDa species **(Figure 7A, Figure S8A)**. Although I211 was barely detectable on western blots containing other ectopically expressing cells due to adjustments made by imaging software, I211 levels were significantly increased compared to untransfected (UT) cells and appeared as a single species rather than a doublet, demonstrating that the Ile start site is capable of translation in this plasmid context, but less efficiently **(Figure 7B, Figure S8B)**. Thus, we used the M211 plasmid for subsequent experiments. Through immunofluorescence microscopy analysis, we observed that hPANX1 WT exhibited prominent cell surface localization with some intracellular staining, whereas we identified a predominantly intracellular localization for M143, M165, and M211. However, the I211 construct exhibited low transfection efficiency and faint intracellular expression **(Figure 7C, Figure S7B, Figure S8C)**. The localization findings for I211 and M211 were in agreeance with MemPype predictions since hPANX1 I211-C426 scored highly in the internal membrane score parameter (**Figure S6A**). In the WT and M211 co-expression condition, staining was observed at both the plasma membrane and intracellularly (**Figure 7C**).

To assess for any co-localization with hPANX1 and M211, we used a PANX1 NT antibody which can detect full length hPANX1 but not endogenous hPANX1-25K or M211 and an HA antibody which can only detect the HA-tagged M211. Interestingly, two smaller immunoreactive species containing the PANX1 NT epitope were also present **(Figure 7D)**. Similar to the PANX1 CT antibody immunofluorescence results, we found hPANX1 WT exhibited both cell surface and intracellular localization while M211 appeared to be solely intracellular **(Figure 7E)**, with perinuclear co-localization of WT and M211 in structures reminiscent of the Golgi apparatus. Co-

immunoprecipitation of WT and M211 confirmed this interaction in Hs578T *hPANX1* KO cells co-expressing the WT and M211 constructs **(Figure 7F)**, indicating full length hPANX1 and M211 can associate. To determine intracellular localization, cells were co-stained with a variety of organelle markers including protein disulfide isomerase (PDI, endoplasmic reticulum lumen), calnexin (endoplasmic reticulum membrane), Golgi matrix protein 130 (GM130, cis/medial Golgi network), trans Golgi network 46 (TGN46), Ras-related protein 7 (RAB7, late endosome) or lysosomal-associated membrane protein 1 (LAMP1) in addition to an HA or PANX1 NT antibody (**Figure 7G, Figure S9**). We observed a high degree of co-localization between M211 and both GM130 and TGN46, as well as PANX1 WT and TGN46, indicating the interaction between hPANX1 WT and M211 most likely occurs in the Golgi apparatus. M211 also showed strong co-localization with LAMP1 suggesting M211 is also present in lysosomes and may be degraded through this pathway which is common with construct overexpression. Weak co-localization was also observed between endoplasmic reticulum markers and M211.

As our findings suggest that hPANX1-25K exhibits a predominantly intracellular localization, we next determined whether any proportion of hPANX1-25K traffics to the plasma membrane. Cell surface markers wheat germ agglutinin and E-cadherin were used to outline the plasma membrane in M211 or WT and M211 expressing Hs578T *hPANX1* KO cells **(Figure S10A, B**, **Figure S11)**, and M211 expressing SCC-13 cells **(Figure S10C, D)**, respectively. Cell surface line scans revealed that although not commonly seen, a subpopulation of M211 can reach the plasma membrane. Cell surface biotinylation in SCC-13 cells was consistent with the immunofluorescence analysis, demonstrating that a small subpopulation of hPANX1-25K is present at the cells surface but only when M211 is overexpressed **(Figure S10E)**. Endogenous hPANX1-25K is solely intracellular, suggesting that there may be a biological relevance to retain hPANX1-25K away from the plasma membrane in these cancer cells.

hPANX1-25K is high mannose glycosylated, can interact with β-catenin, and has two additional N-glycosylation sites on the C-terminus domain similar to full length hPANX1

Since hPANX1-25K is predicted to retain many of the protein modification and interaction sites of hPANX1, we sought out to characterize hPANX1-25K biochemically to see if this isoform contains similar post-translational modifications. First, to assess N-linked glycosylation, we treated lysates from Hs578T *hPANX1* KO cells co-expressing hPANX1 WT and M211 with

PNGase F which removes all N-linked glycans. We saw a complete shift in all hPANX1 and M211 bands to the lowest molecular weight species indicating that M211 is glycosylated when ectopically expressed **(Figure 8A)**. To further characterize the glycan content, we treated the same lysates with Endoglycosidase H (Endo H) which cleaves only N-linked high mannose glycosylation. M211 exhibited only a partial digestion into the de-glycosylated form, even when the amount of enzyme was doubled **(Figure 8A)**, suggesting a portion of hPANX1-25K receives complex glycosylation but most of the species contain only high mannose glycans. However, when we subjected endogenous lysates from SCC-13 (**Figure 8B**) and 131/4-5B1 (**Figure 8C)** cancer cell lines to PNGase F treatment we saw no detectable hPANX1-25K band shifts upon de-glycosylation treatment. In order to test if these endogenous bands were also N-glycosylated, we immunoprecipitated both hPANX1 and hPANX1-25K from 131/4-5B1 cell lysates and analyzed them by mass spectrometry followed by Glycan Finder software (Bioinformatics Solutions Inc.). As expected, both isoforms had N-glycosylated peptides at the canonical N255 site. Surprisingly, we also detected several N-glycosylated peptides at N338 and N394 in the predicted C-terminal (CT) tail of both protein isoforms with 6-8 peptides flanking each amino acid position (**Figure 8D, E; Figure S12**). Interestingly, despite being predicted to contain the same amino acid sequence as the full length hPANX1 (1-426), the NetNGlyc 1.0[54] consensus site predictions for N-linked glycosylation potential were slightly higher for the predicted amino acid sequence of hPANX1-25K (211-426), with N255, N338 and N394 sites scores above the potential threshold of 0.5 **(Figure 8F, G)**. These results give us high confidence that hPANX1-25K is not only a novel isoform of hPANX1, but is also highly glycosylated at previously predicted but unreported sites of N-linked glycosylation.

We previously found that the CT tail of hPANX1 can interact directly with β-catenin [55]. Our co-immunoprecipitation analyses, in both 131/4-5B1 melanoma cells which contain both full length hPANX1 and hPANX1-25K as well as Hs578T *hPANX1* KO breast cancer cells which are devoid of full length hPANX1, determined that hPANX1-25K is also able to complex with β-catenin **(Figure 9A, B)**. Overall, these findings indicate that hPANX1-25K post-translational modifications and interacting partners resemble that of hPANX1.

hPANX1-25K is upregulated in human cSCC tumours compared to normal skin

Since hPANX1-25K appears to be prominent in cancer cell lines and may be differentially regulated in skin cancer compared to normal keratinocytes *in vitro* **(Figure 4)**, we sought to investigate whether this was also seen in human cutaneous tumours and skin tissue. In human melanoma tumours, hPANX1-25K was present at all stages of disease progression **(Figure 9C)**, with no significant differences observed between melanoma tumour fragments from primary, nodal, and distant metastases. Similar to findings in cell lines, we saw that hPANX1-25K levels were also significantly increased in patient-derived cSCC tumour fragments compared to patient-matched normal skin, with the ratio of hPANX1-25K to full length hPANX1 trending towards an increase **(Figure 9D)**. Collectively, these findings suggest that both hPANX1 and hPANX1-25K are upregulated in cancerous skin cells.

DISCUSSION

PANX1 is upregulated in many cancer types where channel activity and protein interactions facilitate the formation and progression of tumours[1-3], and in breast cancer, the truncated PANX1[1-89] mutant confers a metastatic advantage through augmented ATP release[11,56]. Other PANX1 transcript isoforms have been documented in rodents and humans[18], but little is known about the localization and functions of PANX1 isoforms in disease states such as cancer where canonical transcription and translation is often compromised[28,57]. Here, we report the initial identification and characterization of hPANX1-25K, which is intracellularly localized, N-glycosylated and biochemically similar to full length hPANX1. This novel hPANX1 isoform, together with hPANX1, are present at higher level in cutaneous patient tumours and cancer cell lines where they may promote cancer cell growth and survival.

Our results suggest that the *hPANX1* ATC sequence corresponding to I211 is likely the hPANX1-25K start site since hPANX1-25K matches the predicted molecular weight of the fragment from 211-426. Furthermore, hPANX1-25K likely arises from alternative translation of the full length *hPANX1* transcript since we could not identify any alternate promoter start sites or transcript variants which would account for a hPANX1 isoform of that size in our own analysis, and that hPANX1-25K is detected by antibodies targeting PANX1 CT but not NT, as well as the lack of NT peptides detected in our MS analysis. We also saw that hPANX1-25K levels are negatively correlated with hPANX1 and increase with *hPANX1* M1 start site ablation in three different cell lines. This points to an ATI mechanism of leaky ribosome scanning[38] being

potentially responsible for hPANX1-25K upregulation, whereby ribosomes would scan past the initial 5' AUG site of the full length *hPANX1* transcript in favour of downstream internal start sites such as I211. To further investigate the possibility of hPANX1-25K as an ATI hPANX1 isoform beginning at I211, future studies should perform ribosome sequencing of the *hPANX1* transcript to positively identify internal translation start sites present throughout the mRNA. However, we recognize that the transcriptomic analysis may not be representative of the cell lines used in our own study, and the above results do not preclude hPANX1-25K from being produced from alternative transcription, splicing, or promotor usage, meaning we cannot rule out the possibility of a transcript or splice variant. Furthermore, there is evidence of a predicted rat *Panx1* transcript variant X1 (XM_039081351.2) which could produce the predicted rat PANX1 isoform X1 (XP_038937279.1) that includes rat PANX1 residues M210-C426[19]. This variant has not been confirmed at the protein level, but the sequence spans the exact residues we predict for hPANX1-25K. Deep RNA sequencing would be needed to identify a potential hPANX1-25K transcript, especially if the transcript is expressed at low levels[58]. Lastly, we did not find any evidence of human protease consensus sites in hPANX1 which would produce a 25 kDa hPANX1 fragment, and to our knowledge, no non-caspase protease consensus sites have been previously reported in the hPANX1 protein sequence. hPANX1 contains two caspase cleavage sites at aspartic acid residues D167[59] and D379[43] which would produce CT fragments detectable by the PANX1 CT-412 antibody used in our study. However, neither cleavage product would correspond to the ~25 kDa molecular weight of the hPANX1-25K isoform since cleavage at D167 would produce a slightly larger CT fragment (~29.1 kDa), whereas proteolysis at D379 would produce a shorter product (~5.2 kDa). It is also unlikely that hPANX1-25K arises from a cleavage product of full length hPANX1 since hPANX1-25K is increased in HEK, Hs578T, and GBM17 *hPANX1* KO cells, meaning that because hPANX1 is absent, hPANX1-25K cannot be cleaved from the full-length protein. However, examining the origin of the 25K isoform is beyond the scope of this first report and more experimentation is needed.

We initially included I211 as a potential internal start site in our analysis since it corresponds to a Met in mice (M210), but recognize it constitutes an alternative non-AUG start. Although mammalian proteins starting with Ile are rare, one well-known example is the transcriptional enhancer factor TEF-1 (also known as TEA domain family member 1 TEAD1) which is endogenously translated beginning at an AUU start codon which also encodes Ile[60]. New

evidence suggests that translation initiation events at near-cognate codons are much more common than initially believed, accounting for up to 50% of initiation, even though translation from non-AUG codons such as AUC is generally less efficient[39,61]. In the context of cancer, mutations can occur which facilitate alternative mechanisms of translation in cells, with many proto-oncogenes, transcription factors, and growth factors exploiting non-AUG starts to upregulate these tumorigenic proteins[28,62]. Furthermore, alternative translation driven by the non-classical translation initiation factor eIF5A has been shown to promote cancer cell aggressiveness and lung metastasis[63]. Although the *hPANX1* mRNA sequences flanking the I211 'AUC' start site do not completely match a Kozak consensus sequence[42]—which can be a considerable influence for translation initiation efficiency for non-AUG codons[39,61]—there may be other factors to facilitate this internal translation. For example, mRNA structure adjacent to the start site, or non-AUG translation-promoting eukaryotic initiation factors which are increased in cancer, are common mechanisms employed by cells to promote non-AUG translation[39,62,64], but both would need to be investigated further in the case of *hPANX1* mRNA. Additionally, based on previous research replacing the initial AUG start codon of the enzyme dihydrofolate reductase with near-cognate codons, a Met-loaded initiator tRNA may still begin the nascent polypeptide even if the start site encodes a non-Met amino acid[65]. Top-down proteomics in which an intact protein is fragmented[66] could shed light on the specific amino acid sequence and molecular weight of hPANX1-25K.

There are many possibilities for the function of hPANX1-25K as a novel proteoform in mammalian cells and in the context of cancer. hPANX1-25K localizes predominantly to the Golgi network where it interacts with full length hPANX1, rarely trafficking to the cell surface unless induced by overexpression. This is similar to GJA1-20k, which localizes to the endoplasmic reticulum and Golgi apparatus where it associates with Cx43 but does not reach the cell surface to be incorporated into gap junction plaques[30,31,38]. Thus, similar to GJA1-20K and Cx43, hPANX1-25K may interact with full length hPANX1 at the Golgi network to autoregulate its oligomerization and trafficking within the cell. On the contrary, we have observed in melanoma cells that there is increased abundance of intracellular hPANX1 rather than at the plasma membrane[6,8], so it is possible that instead of aiding full length hPANX1 trafficking to the cell surface, hPANX1-25K binds to hPANX1 to sequester the protein intracellularly. Moreover, since the protein may contain multiple transmembrane domains, it is possible that hPANX1-25K oligomerizes to form a channel. However, based on the electrophysiology data obtained with the mouse expression constructs, we

would expect that only M1 and M37 are able to form functional channels on their own. It is more likely that the hPANX1-25K isoform could intermix with full length PANX1 to change the structure and activity of the mixed channel similar to the PANX1$^{1-89}$ mutant[11,56]. Future studies should investigate which domains of hPANX1 full length and hPANX1-25K interact and the potential relative stoichiometry of each hPANX1 form in a mixed channel. Hypothetically, a channel containing hPANX1-25K could be hyperactive since this isoform lacks the NT domain thought to be critical for channel gating[67], which would be advantageous to cancer cells since channel inhibition via PANX1 channel blockers carbenoxolone, probenecid and spironolactone reduce cancer cell properties such as growth, migration, invasion and epithelial to mesenchymal transition in multiple cancer types[6,12,15]. However, the proposed NT-mediated gating mechanisms, either through obstructing a small-ion-permeating side tunnel[68] or rearranging NT conformation within the PANX1 permeation pathway[69] should be revisited. Given that the NT-omitted M37-only form of mPANX1 can be still activated by reversible (**Figure 2E**) and irreversible (**Figure 2D**) mechanisms, and that M37-only(TEV) and TEVp co-expression resulted in whole-cell currents with a similar I-V curve to the CT-cleavage-activated full-length channels, the unidentified PANX1 gating apparatus is likely found between M37 and M372 residues of PANX1. Lastly, through its interaction with the full length hPANX1 channel, hPANX1-25K could either enhance or inhibit binding of protein interactors to hPANX1. This may have signalling consequences in cells, especially in cancers such as melanoma where full length hPANX1 functions in Wnt signalling through its direct interaction with β-catenin to drive melanoma cell metabolism and proliferation[8]. It is evident that the presence of both hPANX1 and hPANX1-25K are favoured in tumours since we observed that hPANX1 and hPANX1-25K are present at high levels in all stages of patient-derived melanoma tumours, and increased in cSCC tumours compared to normal skin[6,70].

When using six different prediction tools to predict hPANX1-25K topology, four platforms reported topologies similar to findings by Spagnol *et al.* for mPANX1[71], indicating a potential membrane-interacting region within the cytoplasmic CT tail. This study determined mPANX1 CT residues I360-G370 may constitute a potential membrane interacting segment because they are predicted to form α-helices by transmembrane domain predicting algorithms[71]. These residues are mostly conserved in hPANX1 (I361-G371), and our own analyses indicated the membrane interacting region corresponds to the hPANX1 residues flanking L370. Our MemPype analysis

predicted another possibility for hPANX1-25K topology, where the protein transverses the membrane once with cytoplasmic NT and extracellular facing CT domains. Interestingly, the residues constituting the MemPype predicted transmembrane domain (L268-L296) does not match that for the canonical hPANX1 transmembrane domain 3 (L218-S239). Further research is needed to confirm the structure and sequence of hPANX1-25K. Intriguingly, we could observe additional N-glycosylated peptides in the CT of both full length hPANX1 and hPANX1-25K isoforms via mass spectrometry. These N-glycosylation sites had been predicted before by us and other groups[40,41,72,73] but had been dismissed as unlikely, given the intracellular topology predicted for the CT of PANX1. Given the conclusive nature of the mass spectrometry identification, we propose that the topology of both hPANX1-25K and hPANX1 full length should be carefully examined since all three of these glycosylation sites may be exposed to the N-glycosylation machinery at different times or within different subcellular compartments.

Through mass spectrometry as well as enzymatic and immunoprecipitation assays, we determined endogenous and exogenously expressed hPANX1-25K shows biochemical similarities to hPANX1 full length such as its ability to undergo N-linked glycosylation and interact with β-catenin. This is in agreement with the prediction that hPANX1-25K is an isoform originating from canonical *hPANX1* beginning at the AUC corresponding to I211, since hPANX1-25K would retain an identical protein sequence and corresponding modification and protein interaction sites present after the I211 residue. As such, we speculate that the CT tail of hPANX1-25K most likely interacts with the NT of β-catenin as with full length hPANX1[8] since we saw the association of hPANX1-25K to β-catenin in cells with and without full length hPANX1 present. Post-translational modification of hPANX1 such as glycosylation and phosphorylation have been shown to alter channel trafficking[41,72] and activity[46,47], respectively, which may also occur in the case of hPANX1-25K. To this end, Endo H and PNGase F digestion of M211 determined a large proportion of this isoform contains high mannose glycans, but a small fraction is further modified to complex glycosylation. This is supported by M211 being found predominantly in intracellular compartments including the Golgi network, corresponding to the high mannose Gly1 species of hPANX1 full length which is present in the endoplasmic reticulum and early Golgi apparatus. In the same way, a small fraction of M211 reaches the plasma membrane similar to hPANX1 Gly2 which is complexly glycosylated and predominantly found at the cell surface[41,72].

To our knowledge, this is the first report and characterization of the hPANX1-25K isoform that may act as a regulator of the full length hPANX1 channel and its downstream signalling in cancer. Our results emphasize the importance of investigating additional isoforms of PANX1, considering that isoforms such as hPANX1-25K will change the landscape of what is known about PANX1 biochemistry, trafficking, and function. Furthermore, these isoforms and their interactions may present novel targets for therapeutic intervention in cases where their levels or activity are altered during cancer progression, and likely other diseases.

ACKNOWLEDGEMENTS

We would like to thank Dr. Aaron Grant and Dr. Steven Latosinsky (London Regional Cancer Program) and their patients which provided melanoma samples for the study. Likewise, we thank Dr. Kathryn Roth's and Dr. Matthew Hebb's patients for providing the skin and cSCC tumours, and GBM tumour samples, respectively. We would also thank Dr. Samy Lamouille (Virginia Tech) and Dr. Michael Koval (Emory University) for their feedback and suggestions for the study. This work was supported by Canadian Institutes of Health Research CIHR Project grants (FRN 153112 to S.P. and 185953 to S.P., M.H. and J.R.), a United States National Heart, Lung, and Blood Institute grant (P01 HL120840) to D.A.B., and a Synthego Genome Engineer Innovation Grant to J.J.K.

AUTHOR CONTRIBUTIONS

Conceptualization: B.O'D., M.J.Z., D.J., L.G., S.S., J.W.S., Y-H.C., D.A.B., S.P.; Data Curation: D.S., M.J.Z. Y-H.C.; Formal Analysis: B.O'D., D.S., M.J.Z., J.T., S.E.L., L.G., Y-H.C.; Funding Acquisition: D.A.B., S.P., J.J.K.; Investigation: B.O'D., D.S., M.J.Z., J.T., D.J., S.E.L., T.J.F., J.J.K., K.B., S.S., Y-H.C.; Methodology: B.O'D., D.S., M.J.Z., S.E.L., D.J., L.G., J.J.K., J.W.S., Y-H.C., D.A.B., S.P.; Project Administration: B.O'D., D.J., L.G., S.P.; Resources: D.W.L., K.R., J.W.S., M.H., J.R., D.A.B., S.P.; Supervision: B.E.I., D.W.L., K.R., J.W.S., M.H., J.R., D.A.B., S.P.; Visualization: B.O'D., D.S., M.J.Z., J.T., S.E.L., C.VK., Y-H.C.; Writing – original draft: B.O'D., M.J.Z., Y-H.C., S.P.; Writing – review and editing: all authors.

DECLARATION OF INTERESTS

The authors declare no competing interests.

FIGURE LEGENDS

Figure 1. Multiple glycosylated forms of mPANX1 proteins are expressed from different translational initiation sites. (A) Schematic depicts predicted molecular weights (in kDa), topology and post-translational modifications of potential mPANX1 ATI isoforms starting at each internal methionine (M) residue. **(B)** Western blots show that transiently expressing HA-tagged mPANX1 (mPANX1-HA) in HEK293T cells produced multiple protein species of varying sizes which were sensitive to PNGase F treatment. **(C)** Sequence alignments showed that the *mPANX1* transcript encodes multiple in-frame methionine residues, including M1, M37, M143, M210 and M374, that follow the Kozak initiation consensus sequence (RxxAUGG; R=A/G). Key residues matching the Kozak consensus sequence (first row) are shown in red. Different Kozak sequences were used in the *mPANX1* transcript (Acc) and the construct encoding HA-tagged mPANX1 (Gcc) at the M1 site. **(D)** Western blotting shows HEK293T cells transfected with wildtype mPANX1-HA (WT), shorter PANX1 isoforms from each internal start site (M1, M37, M143, M210, M374 Only) or empty vector (Mock) constructs and subjected to PNGase F treatment. Arrows indicate varying forms of mPANX1 proteins which matched predicted protein sizes and were sensitive to PNGase F-mediated deglycosylation. M374 was not detected. Tubulin used as protein loading control, protein sizes in kDa.

Figure 2. mPANX1 ATI isoforms traffic to the cell surface, but only the M37-only channels are activated by C-tail cleavage or α1-adrenoceptor stimulation. (A) Western blotting shows HEK293T cells transfected with wildtype mPANX1-HA (WT), shorter mPANX1 isoforms from each internal start site retaining only one in-frame methionine (M1, M37, M143, M210 Only) or empty vector (Mock) constructs. All mPANX1 isoforms were found to be capable of trafficking to the plasma membrane via cell surface biotinylation. Tubulin used as protein loading control, protein sizes in kDa. **(B)** Whole-cell recordings were carried out in HEK293T cells transiently transfected with each mPANX1 isoform as indicated. Bracketed numbers show the number of cells recorded in each group. Inset: an exemplar whole-cell current of M1-only mPANX1, before (basal) and after bath application of 50 μM carbenoxolone (CBX). **(C)** CBX-sensitive whole-cell currents of WT or M1-only mPANX1 were normalized to its peak current at +80 mV. **(D)** Exemplar

current-voltage (I-V) relationships of whole-cell recordings carried out in HEK293T cells co-expressing red fluorescent proteins (RFP) with either M37-only(Tobacco Etch Virus, TEV) and TEV protease (TEVp, left), M37-only(TEV) (middle), or M37-only and TEVp (right). Currents before and after the application of 50 μM CBX are shown as the black and red lines, respectively. **(E)** Time series of exemplar whole-cell recordings of HEK293T cells expressing the M37-only form of mPANX1, with (middle) or without (left) co-expression of mouse α1D adrenoceptors. The I-V relationship of whole-cell currents (right) was obtained from a HEK293T cell co-expressing the M37-only form of mPANX1 and mouse α1D adrenoceptors, under basal conditions (black line), after bath application of 20 μM phenylephrine (+PE; blue line) or after addition of 50 μM CBX (+CBX, red line).

Figure 3. hPANX1 structure and potential internal translation start sites. (A) Schematic depicts hPANX1 topology, post-translational modifications, sites of antibody binding and internal methionine (M) and isoleucine (I) amino acid residues which could act as potential internal start sites. **(B)** Table depicts hPANX1 topology, amino acid (aa) length and predicted molecular weight in kDa for potential ATI isoforms. Created using Adobe Illustrator CS6. **(C)** Kozak consensus sequence assessment for potential internal translation start sites of *hPANX1* mRNA shows multiple in-frame Met and one Ile that follow the Kozak initiation consensus sequence (RxxAUGG; R=A/G). Key residues matching the Kozak consensus sequence (first row) are shown in red. **(D)** Immunoblotting of Hs578T *hPANX1* KO cells expressing wildtype (WT) hPANX1 showed protein species of varying sizes smaller than full length hPANX1. Blot probed with PANX1 CT-412 antibody.

Figure 4. hPANX1-25K is present in many established and patient-derived human cell lines and differentially regulated in normal and cancer cells. Immunoblotting using osteosarcoma, melanoma, breast cancer **(A)** and glioblastoma multiforme (GBM) **(B)** established and patient-derived cell lines. Patient-derived melanoma cell lines were isolated from primary (P), nodal metastasis (N) and distant metastasis **(**D**)** tumours. Western blot indicates presence of hPANX1-25K in all cell lines. **(C)** Immunoblotting assessed hPANX1-25K in N/TERT-1 keratinocyte and squamous cell carcinoma SCC-13 cells. Quantifications showed hPANX1-25K and the ratio of hPANX1-25K to full length hPANX1 is increased in SCC-13 compared to N/TERT-1 cells (*N*=4,

$p<0.01$). SCC-13 cells ectopically expressing full length hPANX1 (SCC-13 + hPANX1) as positive control. Unpaired t test. Bars indicate mean ± SEM. All blots probed with PANX1 CT-412 antibody, with GAPDH as protein loading control. Protein sizes in kDa. **(D) Genomic sequencing of cell lines. The DNA nucleotides 'ATC' encoding isoleucine are present in the location corresponding to amino acid 211 in all cell lines which matches the hPANX1 NCBI RefSeq (NG_027936.1). Dots represent conserved nucleotides. **(E)** Schematic depicts possible topology for hPANX1-25K including sites of post-translational modifications and PANX1 CT-412 antibody binding based on that of the canonical hPANX1 with the protein beginning at the predicted hPANX1-25K start site at I211. Created using Adobe Illustrator CS6.

Figure 5. CRISPR/Cas9 deletion of full length *hPANX1* increases hPANX1-25K, which is not detectable with N-terminal PANX1 antibodies. Immunoblotting using wildtype (WT) and full length *hPANX1* partial or complete knockout (KO) in HEK293T **(A)**, Hs578T **(B)** and GBM17 **(C)** cells. Blots probed with PANX1 CT-412 antibody. Quantifications for HEK293T **(D)**, Hs578T **(E)** and GBM17 **(F)** cells show increases in hPANX1-25K levels with full or partial deletion of *hPANX1* and significant negative correlations between the levels of hPANX1 and hPANX1-25K (*$p<0.05$, **$p<0.01$). **(C)** hPANX1-25K is not detectable in HEK293T **(G)**, Hs578T **(H)** and GBM17 **(I)** WT or *hPANX1* KO cells in western blots probed with PANX1 N-terminal antibodies (NT). GAPDH as protein loading control. Protein sizes in kDa. Unpaired t test and correlations for HEK and Hs578T cells, ordinary one-way ANOVA and nonlinear regression for GBM17 cells. RT-qPCR of HEK **(J)**, Hs578T **(K)** and GBM17 **(L)** WT and *hPANX1* KO cells shows no significant differences in the levels of *hPANX1* transcript. *GAPDH* was used to calculate normalized mRNA using the ΔΔCT method. Unpaired t tests. Guide RNA targeted the beginning of exon 1 in CRISPR-Cas9 deletion of full length *hPANX1*. Bars indicate mean ± SEM. $N=3$.

Figure 6. hPANX1-25K is an isoform of hPANX1 devoid of NT peptides. (A) Immunoprecipitation using PANX1 CT-412 antibody in 1 mg of 131/4-5B1 protein lysates. Samples for GelCode Blue staining and western blotting were run in parallel in the same gel. Full length hPANX1 (pink rectangles) and hPANX1-25K (yellow rectangles) locations were determined in western blot and the matching bands were excised from the GelCode Blue stained gel to send for mass spectrometry identification. Rabbit immunoglobulin G (IgG) pulldown as

negative control. Unspecific bands in gel due to IgG antibody fragments. **(B)** hPANX1 peptides detected by mass spectrometry (blue lines) from the hPANX1-25K band. The identified peptides are mapped to the full length hPANX1 amino acid sequence (grey outlining of residues showcases peptide fragment coverage). Corresponding mass spectrometry spectra for each identified peptide is also shown. Green 'O' indicates sites of oxidation at methionine residues. Red 'C' indicates sites of cysteine carbamidomethylation. Images exported from PEAKS® Studio 11 software.

Figure 7. Overexpression of M211 demonstrates intracellular localization and association with hPANX1. (A) Western blotting using PANX1 CT-412 and HA antibodies shows Hs578T full length *hPANX1* KO cells transfected with wildtype hPANX1 (WT), the shorter HA-tagged I211 or M211 hPANX1 isoforms or co-expression of the WT and M211 constructs compared to untransfected (UT) controls 48 h post-transfection. **(B)** Immunoblotting at increased scanning intensity indicates hPANX1-25K is significantly increased (*p<0.05) with I211 transient transfection compared to UT Hs578T full length *hPANX1* KO cells. Unpaired t test. Bars indicate mean ± SEM. **(C)** Merged immunofluorescence images of the hPANX1 isoform plasmids in Hs578T full length *hPANX1* KO cells. Coverslips probed with PANX1 CT-412 (green). **(D)** Immunoblotting shows hPANX1 WT but not M211 is detectable by PANX1 NT antibodies. GAPDH as loading control, protein sizes in kDa. **(E)** Confocal micrographs show hPANX1 WT (green, PANX1 NT) and M211 (red, HA) co-localization (yellow) in WT and M211 co-expressing Hs578T full length *hPANX1* KO cells. **(F)** hPANX1 and M211 interact as shown by co-immunoprecipitation in WT, M211 expressing Hs578T full length *hPANX1* KO cells using PANX1 NT (hPANX1) and HA (M211) antibodies. Rabbit and mouse immunoglobulin G (IgG) pulldown used as negative controls. Unspecific bands due to IgG antibodies in control and Protein G beads. **(G)** Confocal micrographs of WT, M211 co-expressing Hs578T *hPANX1* KO cells show co-localization of M211 (HA) in green with Golgi apparatus markers GM130 and TGN46 (red). Nuclei in blue counterstained with Hoechst 33342. Scale bars represent 10 µm. N=3 for all experiments.

Figure 8. hPANX1-25K and hPANX1 are N-glycosylated at the canonical N255 and novel N338 and N394 sites. (A) Both hPANX1 WT and M211 in Hs578T *hPANX1* KO cells co-expressing WT, M211 constructs are sensitive to PNGase F treatment via western blot. Endo H

digestion of Hs578T *hPANX1* KO cells co-expressing WT, M211 indicates partial digestion of M211 even when the amount of enzyme was doubled (++). Endogenous hPANX1-25K is resistant to PNGase F treatment, in both SCC-13 **(B)** and 131/4-5B1 **(C)** cells. GAPDH as protein loading control, protein sizes in kDa. *N*=3. hPANX1-25K **(D)** and hPANX1 **(E)** glycopeptide sequence coverage (light green) from 131/4-5B1 cells detected by mass spectrometry, mapped onto a topological depiction of the hPANX1 sequence (generated using Protter 1.0). Asparagine (N) residues in dark green denote glycosylation sites, hPANX1-25K predicted start site (I211) denoted in pink. NetNGlyc 1.0 predicted N-linked glycosylation consensus sites for hPANX1 for residues 211-426 **(F)** and 1-426 **(G).**

Figure 9. hPANX1-25K interacts with β-catenin, is present throughout melanoma disease progression, and increased in cSCC tumour fragments compared to healthy skin. Like hPANX1, hPANX1-25K interacts with β-catenin as shown by co-immunoprecipitation using PANX1 CT-412 and β-catenin antibodies in 1 mg of 131/4-5B1 **(A)** and Hs578T *hPANX1* KO **(B)** protein lysates. Rabbit and mouse immunoglobulin (IgG) pulldown as negative controls. Unspecific bands due to IgG antibodies in control and Protein G beads. *N*=3. **(C)** Immunoblotting with primary (*N*=6), nodal metastasis (*N*=6) and distant metastasis (*N*=3) melanoma tumours shows hPANX1-25K is detectable throughout disease progression where its levels do not change between tumour types (ns, not significant, $p>0.05$). Ordinary one-way ANOVA. **(D)** Representative western blot for hPANX1-25K levels in patient-matched normal skin (S, minus hypodermis) and cutaneous squamous cell carcinoma (cSCC) tumour fragments (T). *N*=17, each # corresponds to a different patient. Quantifications showed hPANX1-25K is significantly increased (***$p<0.001$) and the ratio of hPANX1-25K to hPANX1 trends to an increase ($p=0.1329$) in cSCC tumours compared to skin. GBM17 cells as positive control (+). Unpaired t test. Bars indicate mean ± SEM. Blots probed with PANX1 CT-412 antibody, GAPDH as protein loading control. Protein sizes in kDa. Bars indicate mean ± SEM.

TABLES

Table 1. Primers used for generating Met-to-Ile mutations and (TEV) in mPANX1.

Mutation	Forward Primer 5'-3'	Reverse Primer 5'-3'
M1I	TGCGCCTTGACCATTGCCATCGC CCACTTG	CAAGTGGGCGATGGCAATGGTCA AGGCGCA

M37I	GGTGGACAAGATCGTCACATGTATTG	CAATACATGTGACGATCTTGTCCACC
M143I	CCTGAAGTTTATCATCGAGGAACTTGAC	GTCAAGTTCCTCGATGATAAACTTCAGG
M210I	CTCTAGTCATTTAATCATCAAATACATTAGCTGCCGGCTGG	CCAGCCGGCAGCTAATGTATTTGATGATTAAATGACTAGAG
M374I	GCATGATTAAGATCGACATCATTGATG	CATCAATGATGTCGATCTTAATCATGC
M37-only(TEV)	CTCCTGACAAACCTTGGCATGGAAAACTTGTATTTTCAAGGTGGAAAAATTCCCACGTCCCTA	AGGGACGTGGGAATTTTTCCACCTTGAAAATACAAGTTTTCCATGCCAAGGTTTGTCAGGAG

Table 2. RT-qPCR primers.

Target	Forward Primer 5'-3'	Reverse Primer 5'-3'
hPANX1	CCCTGGACCGGATAGTCAAG	CGGATGCTGAAGTTACTGGGA
GAPDH	AATCCCATCACCATCTTCCA	TGGACTCCACGACGTACTCA

MATERIALS AND METHODS

PANX1 sequence analysis

NCBI RefSeq mRNA and protein sequences of mPANX1 (mRNA NM_019482.2, protein NP_062355.2) and hPANX1 (mRNA NM_015368.4, protein NP_056183.2)[19] were analyzed to identify potential internal Met and Ile start sites downstream of the canonical M1 site. mRNA sequences of mPANX1 and hPANX1 were translated using Expasy[52] to visualize the protein sequence which allowed us to identify neighbouring amino acid residues and corresponding codons of predicted Met and Ile start sites to compare to the Kozak consensus sequence[42]. Protein sequence homology was compared using NCBI standard protein BLAST, inputting hPANX1 protein as the query sequence. Aligned sequences were compared between hPANX1 and relevant organisms with available complete PANX1 sequences and included based on phylogenetic relevance and sequence homology to *Homo sapiens*. Theoretical molecular weights were calculated using the Expasy[52] Compute pI/Mw (isoelectric point/molecular weight) Tool (https://web.expasy.org/compute_pi/).

Cell culture

HEK293T (ATCC CRL-3216, RRID:CVCL_0063), HEK293T *PANX1* KO[55], REK (gifted from Dr. Dale Laird, University of Western Ontario, London, ON), A375-MA2 (ATCC CRL-3223,

RRID:CVCL_X495), Hs578T (ATCC HTB-126, RRID:CVCL_0332), Hs578T *PANX1* KO[55], A2058 (ATCC CRL-11147, RRID:CVCL_1059), C8161 (gifted from Dr. Lynne-Marie Postovit, Queen's University Kingston, ON; RRID:CVCL_6813), U-2 OS (ATCC HTB-96, RRID:CVCL_0042), U-87 MG (ATCC HTB-14, RRID:CVCL_0022), U-251 MG (Millipore Sigma 09063001-1VL; RRID:CVCL_0021), LN-229 (ATCC CRL-2611 RRID:CVCL_0393), GBM17, GBM17 *PANX1* KO (generated using the same CRISPR/Cas9 protocol as Nouri-Nejad *et al.*[55]), GBM20, GBM23, GBM29, GBM34 and patient-derived primary, nodal and distant metastasis melanoma[6] cell lines were cultured in DMEM media (Gibco #12430062) supplemented with 10% fetal bovine serum (FBS; Thermo Fisher Scientific #12483020) and 1% penicillin/streptomycin (Gibco #15140-122). 131/4-5B1 cells[74], which were a kind gift from Dr. Lina Dagnino (University of Western Ontario) and originally obtained from Dr. Robert Kerbel (Sunnybrook Health Sciences Centre, Toronto, ON), were cultured in RPMI 1640 media (Gibco #61870036) supplemented with 10% FBS and 1% penicillin/streptomycin. N/TERT-1 cells (RRID:CVCL_CW92) were grown in KGM™ Gold Keratinocyte Growth Medium supplemented with the BulletKit™ (Lonza #00192060) and SCC-13 cells (RRID:CVCL_4029) in DMEM media supplemented only with 10% FBS (WISENT #098-150). N/TERT-1 and SCC-13 cells were gifted by Dr. Lina Dagnino. Cells were maintained at 37°C with 5% CO_2 and confirmed mycoplasma-negative using the MycoAlert® Mycoplasma Detection Kit (Lonza #LT07-318).

Cloning and plasmids

The mPANX1-HA expression vector was a gift from Dr. Kodi Ravichandran[44,45]. The Tobacco Etch Virus protease (TEVp) plasmid was kindly provided by S. R. Ikeda[75], and the pRFP-C1 plasmid was kindly provided by Dr. Julius Zhu (University of Virginia). The mouse α1D adrenoceptor plasmid was obtained from OriGene (#MR222643)[76]. To generate different Met to Ile mutations, site-directed mutagenesis was performed on the mPANX1-HA construct using PfuTurbo polymerase (Agilent #600250) with various combinations of primers **(Table 1)**. To generate the M37-only(TEV) constructs, the CT caspase 3/7 cleavage site of M37-only form of mPANX1 (IKMDIID) was replaced by TEVp recognition sequence (ENLYFQG) using the same site-directed mutagenesis approach as above. The hPANX1 WT plasmid was purchased from InvivoGen (#puno1-hpanx1) and modified by NorClone Biotech Laboratories to create the vectors

encoding the I211 and M211 proteins which were tagged with HA on the CT. All constructs were verified by using Sanger's sequencing.

Transfection

Transient transfections were performed using Lipofectamine™ 2000 (Invitrogen #11668027) for all mouse plasmids and Lipofectamine™ 3000 (Invitrogen #L3000015) for all human plasmids. For immunoblotting and cell surface biotinylation of mPANX1, 4 µg and 8 µg of mPANX1 plasmids were used for transfections in a 6-well plate or 6-cm dish, respectively. For whole-cell recordings, cells were co-transfected with 0.9 µg of a plasmid containing mouse adrenergic α1D receptor (OriGene #MR222643)[77] or Tobacco Etch Virus protease (TEVp)[43], 0.3 µg of mPANX1 constructs, and 0.1 µg of EGFP-encoding plasmids (pEGFP-C1) in a 12-well plate. Unless otherwise stated, 0.5 µg of all hPANX1 plasmids (0.25 µg each of hPANX1 WT and M211 in the co-expression condition) were used for transfections in a 6-well plate. Reagents were added to Opti-MEM media (Life Technologies #51985-034) and cells were transfected according to the manufacturer's protocol. Cells were transfected 24 h after seeding and experiments were performed either 24 h or 48 h after transfection as noted.

Protein isolation and immunoblotting

In HEK293T cells overexpressing various mPANX1 plasmids, protein was extracted using a PBS buffer containing 1% Triton X-100, protease inhibitor cocktail (Sigma-Aldrich #P8340), 10 mM NaF, and 10 mM $NaVO_3$. Unless otherwise noted, protein was isolated from human cell lines using 1x RIPA buffer (50 mM Tris-HCl at pH 8.0, 150 mM NaCl, 1% Nonidet™ P 40 Substitute [Sigma-Aldrich #74385], 0.5% sodium deoxycholate), and from human tissue using 2x RIPA buffer after pulverizing in liquid nitrogen. Extraction buffers were supplemented with 1 mM NaF, 1 mM Na_3VO_4 and half of a Pierce Protease Inhibitor EDTA-free Mini Tablet (Thermo Fisher Scientific #A32955). Protein was quantified using a bicinchoninic acid assay (BCA; Thermo Fisher Scientific #23225).

For immunoblotting analyses of mPANX1 plasmids, 50 µg or 60 µg protein samples were separated by SDS-PAGE using an 8% acrylamide gel, transferred onto 0.45 µm nitrocellulose membranes (PerkinElmer, Inc. #NBA085B001EA), and the membranes were blocked with 5% non-fat dry milk dissolved in a tris-based buffer (10 mM Tris, 150 mM NaCl, and 0.1% Tween 20,

pH 7.4) at room temperature for 1 h. HA-tagged mPANX1 isoforms were probed with anti-HA antibody 1:1000 (Cell Signaling Technology #2367, RRID:AB_10691311) and anti-α-tubulin antibody 1:8000 (Sigma-Aldrich #T9026, RRID:AB_477593) as a loading control. Amersham ECL horseradish peroxidase (HRP)-linked secondary antibodies (GE Healthcare #NA931V or #NA9340V, 1:4000–1:8000) and Western Lightning Plus-ECL (PerkinElmer, Inc. #NEL103001EA) were used to visualize immunoreactive signals on Amersham Hyperfilm ECL (GE Healthcare #28-9068-39). Blots were digitized using the Epson Perfection 4990 Photo desktop scanner. Primary antibodies were diluted in 0.1% Tween 20 PBS and incubated overnight at 4°C, and secondary antibodies were dissolved in 0.1% Tween 20 PBS with 5% non-fat dry milk and incubated for 1 h at room temperature.

Western blots for hPANX1 experiments were performed as previously reported[78], loading 40-50 µg to analyze endogenous proteins from all cell types, except for N/TERT-1 and SCC-13 cells where 70 µg was loaded per sample. For Hs578T *hPANX1* KO overexpressing cells, 40 µg per sample was used. For human tissue samples, 50 µg was used for melanoma tumours and 40 µg was used for cSCC tumour and aged skin samples. Protein samples were separated on 10% acrylamide SDS-PAGE gels which were transferred to nitrocellulose membranes using an iBlot Gel Transfer Device (Invitrogen) on P3. After blocking for 1 h at room temperature in 1x PBS with 3% bovine serum albumin (BioShop ALB001.100), most antibodies were incubated overnight at 4°C, except GAPDH and secondary antibodies which were incubated for 1 h at room temperature. Primary antibody working dilutions included: anti-PANX1 CT-412 1:1000[41,72], anti-PANX1 NT 1:1000 (Cell Signaling Technology #91137, RRID:AB_2800167), anti-PANX1 NT 1:125 (Thermo Fisher Scientific #487900, RRID:AB_2532253), mouse anti-β-catenin 1:1000 (BD Transduction Laboratories™ #610154, RRID:AB_397555), mouse anti-HA 1:5000 (Invitrogen #26183, RRID:AB_2533049), rabbit anti-HA 1:1000 (Cell Signaling Technology #3724, RRID:AB_1549585), mouse anti-GAPDH 1:5000 (Millipore Sigma #G8795, RRID:AB_1078991, Burlington, MA), and mouse anti-E-cadherin 1:2500 (BD Transduction Laboratories™ #610182, RRID:AB_397580). Dilutions of 1:10,000 were used for all secondary antibodies, including IRDye-800CW goat anti-rabbit (LI-COR Biosciences #926-32211, RRID:AB_621843), IRDye-800CW goat anti-mouse (LI-COR Biosciences #926-32210, RRID:AB_621842), IRDye-680RD goat anti-mouse (LI-COR Biosciences #926-68070, RRID:AB_10956588) and IRDye-680RD goat anti-rabbit (LI-COR Biosciences #926-68071,

RRID:AB_10956166) immunoglobulin G (IgG) secondary antibodies. All antibodies were dissolved in 3% bovine serum albumin in 0.05% Tween 20 PBS. Blot imaging and protein and molecular weight quantification were performed using the LI-COR Odyssey Infrared Imaging System and ImageStudio software (LI-COR Biosciences). Protein levels were normalized to GAPDH and presented relative to the control mean value.

RNA isolation and RT-qPCR

RNA was isolated using the RNeasy Plus Mini kit (Qiagen #74134) and 50 ng of RNA was reverse transcribed into cDNA using the High-Capacity cDNA Reverse Transcription Kit with RNase Inhibitor (Thermo Fisher Scientific #4374966) as per the manufacturer's protocol in a T100TM Thermal Cycler (Bio-Rad Laboratories). RT-qPCR was performed using the SsoAdvanced Universal SYBR Green Supermix (Bio-Rad Laboratories #1725274) with samples run in triplicate. Transcript levels were normalized to *GAPDH*, presented as relative to the WT or Control mean value and analyzed with the ΔΔCT method in Excel (Microsoft 365). See **Table 2** for list of primers used. Statistical analyses used logarithmic means, but figure graphs were created using geometric means.

Cell surface biotinylation and co-immunoprecipitation

For cell surface biotinylation experiments performed in HEK293T cells expressing different mPANX1 proteins, cells were labeled with 1 mg/ml EZ-Link Sulfo-NHS-LC-Biotin™ (Thermo Fisher Scientific #21335) in PBS for 1 h at 4 °C, 24 h after transfection. The reaction was quenched by incubating the cells in cold PBS containing 100 mM glycine at 4°C for 20 min, then cells were lysed using PBS containing 1% Triton X-100 and a cocktail of protease inhibitors (Sigma-Aldrich #P8340). Biotinylated proteins were collected by incubating cell lysates with streptavidin-agarose beads (Thermo Fisher Scientific #20349) at 4 ºC for 2 hours.

For cell surface biotinylation with untransfected and M211-expressing (5.5 µg plasmid in a 10 cm plate, 24 h after transfection) SCC-13 cells, cells were labeled with 0.4 mg/mL EZ-Link™ Sulfo-NHS-SS-Biotin (Thermo Fisher Scientific #A39258) for 20 min at 4°C with gentle shaking. Biotin was quenched with 100 mM glycine-DPBS without Ca^{2+} and Mg^{2+} for 30 min at 4°C with gentle shaking after two quick 100 mM glycine-DPBS without Ca^{2+} and Mg^{2+} rinses. Cells were then lysed with SDS lysis buffer (1% Triton X-100, 0.1% SDS, 1 mM NaF, 1 mM Na_3VO_4 in

DPBS without Ca^{2+} and Mg^{2+}), and protein was quantified via BCA assay. Biotinylated proteins were separated out of lysates (1 mg per sample) by 4°C overnight incubation with 30 µL of pre-washed Pierce™ Streptavidin magnetic beads (Thermo Fisher Scientific #88816). The next day, the beads were washed twice with 2x IP buffer and once with 1x DPBS without Ca^{2+} and Mg^{2+} using the DynaMag™-2 magnet (Invitrogen #12321D), resuspended in 50 µL of 2x Laemmeli buffer and boiled for 5 min before running in parallel with 70 µg of input lysates on a 10% acrylamide gel. E-cadherin and GAPDH were used as positive and negative controls, respectively, for cell surface trafficking.

For co-immunoprecipitation experiments, cells were lysed using 1x IP buffer (1% Triton X-100, 150 mM NaCl, 10 mM Tris, 1 mM EDTA, 1 mM EGTA, 0.5% Nonidet P-40) supplemented with 1 mM NaF, 1 mM Na_3VO_4 and half of a Pierce Protease Inhibitor EDTA-free Mini Tablet. Co-immunoprecipitation was performed using 1 mg of 131/4-5B1 cells or Hs578T *PANX1* KO cells co-transfected with PANX1 WT and M211 plasmids (2.75 µg of each plasmid in a 10 cm plate, 24 h after transfection), Pierce™ Protein G magnetic beads (Thermo Fisher Scientific #88847) and the DynaMag™-2 magnet. We followed the manufacturer's protocol except that we used 25 µL of beads per sample, incubated the lysate and antibody-bound beads for 30 min at room temperature and dissociated antibodies from beads by incubating beads with 20 µL 50 mM glycine elution buffer and 10 µL 2x Laemmli sample buffer (Bio-Rad Laboratories #1610737) supplemented with 10% β-mercaptoethanol for 10 min at 70°C in a T100TM Thermal Cycler (Bio-Rad Laboratories). The following antibodies were used for immunoprecipitation: anti-PANX1 CT-412 10 µg[41,72], anti-PANX1 NT 1:100 (Cell Signaling Technology #91137, RRID:AB_2800167), rabbit anti-β-catenin 1:100 (Cell Signaling Technology #8480, RRID:AB_11127855) and mouse anti-HA 5 µg (Invitrogen #26183, RRID:AB_2533049). Equal amounts of either rabbit or mouse IgG antibodies (Thermo Fisher Scientific #02-6102, #02-6502) were used as pull-down controls. To try to minimize background due to IgG antibodies, blots were probed using the Quick Western Kit (LI-COR Biosciences #926-69100) and the corresponding antibody dilutions outlined above.

Deglycosylation

To examine whether different forms of mPANX1 were glycosylated, 50 µg or 60 µg of protein lysates were incubated with glycerol (50%) or 7000 U/mg PNGase F (New England Biolabs

#P0704) at 37 ºC for 3 h before SDS-PAGE separation. For analysis of hPANX1-25K glycosylation, 40 µg of SCC-13 protein lysate and 20 µg of lysates from Hs578T *PANX1* KO cells co-transfected with hPANX1 WT and M211 were subjected to 1000 U of PNGase F (New England Biolabs, Inc. #P0704S) at 37°C for 2 h or 1000 U Endo H (New England Biolabs, Inc. #P0702) for 1 h at 37°C. To visualize any shifts in PANX1 banding, lysates from all deglycosylation assays were separated on either 10% or 12% SDS-PAGE gels.

Electrophysiology

Whole-cell recordings were performed at room temperature using an Axopatch 200B amplifier and pClamp10 software (Molecular Devices). Ramp voltage commands were applied at 7 s intervals, with voltage ranging from -130 to 80 mV (0.2 mV/ms) by using the pClamp10 software and a Digidata 1322A digitizer (Molecular Devices). Micropipettes of 3-5 MΩ were pulled from borosilicate glass capillaries (Harvard Apparatus) using a P-97 Micropipette Puller (Sutter Instrument). Bath solution contains 140 mM NaCl, 3 mM KCl, 2 mM $MgCl_2$, 2 mM $CaCl_2$, 10 mM HEPES, and 10 mM glucose (pH 7.3). Internal (pipette) solution was composed of 30 mM tetraethylammonium chloride, 100 mM $CsMeSO_4$, 4 mM NaCl, 1 mM $MgCl_2$, 0.5 mM $CaCl_2$, 10 mM HEPES, 10 mM EGTA, 3 mM ATP-Mg, and 0.3 mM GTP-Tris (pH 7.3). Carbenoxolone (CBX; Sigma-Aldrich #C4790)-sensitive current was defined as the difference in current at +80 mV, before and after applying 50 µM of CBX in bath, and was normalized to cell capacitance (i.e., current density). Phenylephrine (PE; Sigma-Aldrich #P6126)-induced current was determined by the difference in CBX-sensitive current at +80 mV, before and after applying 20 µM of PE in bath.

Transcriptomics

The FANTOM 5 project[48-50] reprocessed data (https://fantom.gsc.riken.jp/5/datafiles/reprocessed/) was used for the CAGE-seq analysis. Transcription start site (CAGE-seq) peaks across the panel of the biological states (samples) were identified by decomposition based peak identification[48], where each of the peaks consists of neighbouring and related transcription start sites. Nanopore long read RNA sequencing[51] of P60 mouse epidermal stem cells, keratinocytes, and HrasG12V; *Tgfbr2* KO mouse squamous cell carcinomas, sequenced on PromethION, were obtained from https://github.com/ugdastider/long_read_paper, and used to visualize *Panx1* transcript isoforms.

Figures were generated using the UCSC genome browser[79] (https://genome.ucsc.edu/index.html).

Cleavage site and topology predictions

The PANX1_Human UniProt[80] FASTA sequence (accession number Q96RD7) was submitted into the Expasy[52] PeptideCutter webserver (https://web.expasy.org/peptide_cutter/) to obtain predicted cleavage sites of all available enzymes and chemicals. Only agents found naturally in humans were included. Proteases that cleaved ±10 residues from hPANX1 residue I211 were subsequently reviewed for physiological relevancy. Given the possibility of pro-peptide cleavages, the full length hPANX1 sequence was further analyzed through the ProP 1.0 webserver[53] (https://services.healthtech.dtu.dk/services/ProP-1.0/) to predict any potential arginine and lysine pro-peptide cleavage sites or signal peptide cleavage sites (integrated with SignalP-3.0). Both servers incorporate predictions based on artificial neural networks and Hidden Markov models. Both the general pro-protein convertase and furin-tag specific cleavage prediction methods were conducted using ProP1.0-SignalP-30.

A FASTA sequence of hPANX1 I211-C426 was created using the aforementioned PANX1_Human UniProt[80] sequence. Sequences were analyzed through topology prediction servers: ΔG Prediction server[81] v1.0 (https://dgpred.cbr.su.se/index.php?p=TMpred), TOPCONs[82] (https://topcons.cbr.su.se/pred/), Dense Alignment Surface[83] (https://tmdas.bioinfo.se/), and SOSUI[84] v1.11 (https://harrier.nagahama-i-bio.ac.jp/sosui/). Further predictions of potential transmembrane topology were conducted with a Python and terminal script using DeepTMHMM[85] v1.0.24 (https://dtu.biolib.com/DeepTMHMM/). Observations of the truncated isoform being an all-alpha membrane protein led to additional predictions using the all-alpha membrane topology prediction server MemPype[86] (https://mu2py.biocomp.unibo.it/mempype).

Sample preparation, bottom-up mass spectrometry data analysis and glycosylation site predictions

Protein was immunoprecipitated from 131/4-5B1 cells using PANX1 CT-412 and rabbit IgG antibodies and separated as above except using pre-cast 10% Mini-PROTEAN® TGX Stain-Free™ Protein Gels (Bio-Rad Laboratories #4568034). Each immunoprecipitation was run in duplicate on the same gel, where half the gel was stained with GelCode™ Blue Protein Stain (Thermo Fisher

Scientific #24594) and the other half was transferred to nitrocellulose membrane for western blotting using the Quick Western kit as outlined above. For GelCode blue staining, the gel was washed with MilliQ water at room temperature three times, for 5 min each, to remove any lint or debris that was stuck to the gel before staining with GelCode blue for 1 h at room temperature. After three quick rinses with MilliQ water, gels were washed overnight at 4°C to increase band clarity, and then stored in 3% acetic acid (diluted in water) at 4°C. Gel bands were excised using a sterile blade and sent to Bioinformatics Solutions, Inc. (Waterloo, Ontario, Canada) for LC-MS/MS analysis.

In-gel digest samples were reduced with 10 mM dithiothreitol (Sigma-Aldrich), and alkylated with 55 mM iodoacetamide (Sigma-Aldrich). The samples were then digested overnight with MS grade trypsin (Promega). Digested peptides were extracted with 5% formic acid and 100% acetonitrile. The products were dried down and kept in -20°C until analysis.

Prior to MS analysis, samples were resuspended in 0.1% formic acid. Each sample underwent division into two equal parts to facilitate both regular proteomic and glycoproteomic analyses. Subsequently, each aliquot was subjected to nanoflow LC using an UltiMate 3000 Chromatography System (Thermo Fisher Scientific) and then introduced into the Thermo Orbitrap Fusion™ Lumos™ Mass Spectrometer (Thermo Fisher Scientific). LC was performed using a constant flow of 0.25 µL/min and a 15 cm reversed-phased column with a 75 µm inner diameter filled with Reprosil C18 (PepSep). Mobile phase A was 0.1% formic acid, and Mobile phase B was 99.9% acetonitrile and 0.1% formic acid. The separation was carried out over 60 min as follows: linearly 4% B to 32% B over 50 min with an increase to 95% B over 0.1 min and held constant for 4.9 min to clean the column. Then the B percentage was set back to 4% in the final 5 min.

Both proteomic and glycoproteomic analyses utilized the same nano liquid chromatography (nLC) setup but differed in MS/MS data acquisition. For proteomic data acquisition, MS/MS data were acquired using the Thermo Orbitrap Fusion™ Lumos™ instrument in data-dependent acquisition mode with a cycle time of 3 s. MS1 scan data were obtained at a resolution of 60,000 (at 400 m/z) within a mass range of 400–1,600 m/z. The automatic gain control (AGC) was set to standard, with an auto maximum ion injection time. The radio frequency (RF) lens was set to 30%. Charge states 2-8 were filtered, and dynamic exclusion was set to 10 s. Isolation for MS2 scans occurred in the quadrupole with an isolation window of 0.7 Da. MS2 scan

data were acquired at a resolution of 30,000 m/z in the Orbitrap, maintaining a standard AGC target and auto ion injection time. The scan range of MS2 was set to auto. Higher energy collisional dissociation (HCD) with a fixed normalized collision energy (NCE) of 30% was utilized for generating MS2 spectra, with one microscan.

Glycoproteomic data acquisition was also performed on the Fusion™ Lumos™ platform. MS1 data were obtained at a resolution of 120,000 (at 400 m/z) within a mass range of 350-1800 m/z, with dynamic exclusion set to 60 s. Precursor prioritization was based on the highest charge state and lowest m/z. The initial round of MS2 scans was conducted at a resolution of 30,000 m/z in the Orbitrap using HCD with 28% NCE, isolated within a 2 m/z window. If specific fragment ions were observed (HexNac 204.0867 m/z; HexNac fragment 138.0545 m/z; HexNacHex 366.1396 m/z), a second round of MS2 scans was triggered on the same precursor. These additional scans were performed at a resolution of 30,000 m/z in the Orbitrap with a 200% normalized AGC target. Stepped HCD was employed at 20-30-40% NCE and the isolation window for the second round of MS2 scans was increased to 3 m/z. Other parameters for glycoproteomic data acquisition remained consistent with those used for proteomic analysis.

MS raw files were processed using either PEAKS® Studio[87,88] v11.5 for proteomic samples or PEAKS® Glycan Finder II[89] for glycoproteomic samples (Bioinformatics Solutions, Inc). The data was searched against the UniProt (https://www.uniprot.org/) reviewed human protein sequence database[80]. Precursor ion mass error tolerance was set to 10 ppm and fragment ion mass error tolerance was set to 0.02 Da. Semi-specific cleavage with trypsin with a maximum of 3 missed cleavages. A fixed modification of carbamidomethylation (+57.02 Da) on cysteine residues were specified. Variable modifications of deamidation (+0.98 Da) on asparagine and glutamine as well as oxidation (15.99 Da) on methionine were specified. The false discovery rate threshold was set to 1% for database searches. Protein feature visualization was done using Protter 1.0[90].

Putative N-linked glycosylation site predictions for hPANX1 full length and hPANX1-25K were determined using the NetNGlyc 1.0 server[54] with a threshold potential of 0.5 (https://services.healthtech.dtu.dk/services/NetNGlyc-1.0/).

Immunocytochemistry

For analysis of hPANX1 isoform localization in Hs578T *PANX1* KO cells, 250,000 cells were plated on glass coverslips (Fisher Scientific #1254580) in a 6-well plate. Twenty-four or 48 h after

transfection, cells were fixed with ice-cold methanol:acetone (5:1, v/v) for 15 min at 4°C after two washes with 1x DPBS without Ca^{2+} and Mg^{2+}. In a humidity chamber, coverslips were blocked with 10% goat serum (Life Technologies #50062Z) for 1 h at room temperature, and then incubated overnight at 4°C with anti-PANX1 NT 1:250 (Cell Signaling Technology #91137, RRID:AB_2800167), anti-PANX1 CT-412 1:500[41,72], rabbit anti-HA 1:500 (Cell Signaling Technology #3724, RRID:AB_1549585) and/or mouse anti-HA 1:500 (Invitrogen #26183, RRID:AB_2533049). All antibodies were diluted in 1% goat serum in 1x DPBS without Ca^{2+} and Mg^{2+}. The next day, coverslips were washed thrice for 5 min using 1x DPBS without Ca^{2+} and Mg^{2+}, probed with 1:700 Alexa Fluor™ 488 goat anti-rabbit (Invitrogen #A-11008, RRID:AB_143165), 1:700 Alexa Fluor™ 488 goat anti-mouse (Invitrogen #A-11029, RRID:AB_2534088), 1:500 Alexa Fluor™ 647 goat anti-rabbit secondary antibody (Invitrogen A-21244, RRID:AB_2535812) and/or 1:500 Alexa Fluor™ 647 goat anti-mouse secondary antibody (Invitrogen #A-21236, RRID:AB_2535805) for 1 h at room temperature. After 5 min 1x DPBS without Ca^{2+} and Mg^{2+} and distilled water washes, coverslips were stained for cell nuclei with Hoechst 33342 (Life Technologies #H3570) diluted 1:1000 in double-distilled water for 5 min at room temperature. Coverslips were mounted with ProLong™ Gold Antifade Mountant (Thermo Fisher Scientific #P36934) and imaged on a ZEISS LSM 800 AiryScan Confocal Microscope (Schulich Imaging Core Facility, University of Western Ontario) with 63x oil magnification and 405 nm (Hoechst 33342), 488 nm (Alexa Fluor™ 488) and 640 nm (Alexa Fluor™ 633, 647) laser lines.

Mouse anti-E-cadherin 1:200 (BD Transduction Laboratories™ #610182, RRID:AB_397580), and Alexa Fluor™ 633-conjugated wheat germ agglutinin (WGA) 1:100 (Thermo Fisher Scientific #W21404) were incubated with coverslips for 1 h at room temperature to label the cell surface of SCC-13 and Hs578T *PANX1* KO transfected cells, respectively. Line intensity profiles of fluorescent images (line scans) were quantified using ImageJ (Fiji)[91] and visualized for overlap of pixel intensities from each channel. Mouse anti-GM130 (BD Transduction Laboratories #610822, RRID:AB_398141; 1:150), mouse anti-TGN46 (Thermo Fisher Scientific #MA3-063, RRID:AB_325484; 1:75), mouse anti-LAMP1 (Thermo Fisher Scientific #14-1079-80, RRID:AB_467426; 1:100) were incubated on coverslips to visualize the cis/medial-Golgi network, trans Golgi network and lysosomes, respectively. Mouse anti-PDI (Enzo Life Science #ADI-SPA-891F, RRID:AB_10615355; 1:150) and rabbit anti-calnexin (Cell

Signaling Technology #2679S, RRID:AB_2228381; 1:100) were used to visualize the lumen and membrane of the endoplasmic reticulum, respectively. Rabbit anti-RAB7 antibody was used to visualize late endosomes (Cell Signaling Technology #9367, RRID:AB_1904103; 1:75). All organelle markers were incubated on coverslips for 1 h at room temperature as previously described[92].

Patient Samples

Subjects provided informed consent to participate in our Health Science Research Ethics Board (HSREB) of Western University and London Health Sciences Centre (London, ON, Canada, HSREB#103381, HSREB#17290) approved studies which were conducted in accordance with the Declaration of Helsinki. Melanoma[6], cSCC (see O'Donnell *et al.* for patient demographics [9]) and GBM tumour identity was confirmed by a pathologist. Normal aged skin was either left over from skin grafts or obtained via punch biopsy. GBM17, GBM20, GBM23, GBM29 and GBM34 cell lines were derived from operative tumour specimens obtained from GBM patient tumours.

Statistics

Statistical analyses were performed using GraphPad Prism 10 software. Statistical tests as well as biological and technical replicates are reported in individual figure legends.

SUPPLEMENTAL INFORMATION

Document S1: Supplementary Figures S1-S12.

REFERENCES

1 Laird, D. W. & Penuela, S. Pannexin biology and emerging linkages to cancer. *Trends in cancer* **7**, 1119-1131 (2021).

2 Panchin, Y. *et al.* A ubiquitous family of putative gap junction molecules. *Current Biology* **10**, 473-474, doi:10.1016/s0960-9822(00)00576-5 (2000).

3 Jiang, J. X. & Penuela, S. Connexin and pannexin channels in cancer. *BMC Cell Biol* **17 Suppl 1**, 12, doi:10.1186/s12860-016-0094-8 (2016).

4 Derangere, V. *et al.* Liver X receptor beta activation induces pyroptosis of human and murine colon cancer cells. *Cell Death Differ* **21**, 1914-1924, doi:10.1038/cdd.2014.117 (2014).

5 Boyd-Tressler, A., Penuela, S., Laird, D. W. & Dubyak, G. R. Chemotherapeutic drugs induce ATP release via caspase-gated pannexin-1 channels and a caspase/pannexin-1-

independent mechanism. *J Biol Chem* **289**, 27246-27263, doi:10.1074/jbc.M114.590240 (2014).
6 Freeman, T. J. *et al.* Inhibition of Pannexin 1 Reduces the Tumorigenic Properties of Human Melanoma Cells. *Cancers (Basel)* **11**, doi:10.3390/cancers11010102 (2019).
7 Cowan, K. N., Langlois, S., Penuela, S., Cowan, B. J. & Laird, D. W. Pannexin1 and Pannexin3 exhibit distinct localization patterns in human skin appendages and are regulated during keratinocyte differentiation and carcinogenesis. *Cell Commun Adhes* **19**, 45-53, doi:10.3109/15419061.2012.712575 (2012).
8 Sayedyahossein, S. *et al.* Pannexin 1 binds beta-catenin to modulate melanoma cell growth and metabolism. *J Biol Chem* **296**, 100478, doi:10.1016/j.jbc.2021.100478 (2021).
9 O'Donnell, B. L. *et al.* Pannexin 1 and pannexin 3 differentially regulate the cancer cell properties of cutaneous squamous cell carcinoma. *J Physiol*, doi:10.1113/JP286172 (2024).
10 Wei, L., Yang, X., Shi, X. & Chen, Y. Pannexin1 silencing inhibits the proliferation of U87MG cells. *Mol Med Rep* **11**, 3487-3492, doi:10.3892/mmr.2015.3169 (2015).
11 Furlow, P. W. *et al.* Mechanosensitive pannexin-1 channels mediate microvascular metastatic cell survival. *Nat Cell Biol* **17**, 943-952, doi:10.1038/ncb3194 (2015).
12 Jalaleddine, N. *et al.* Pannexin1 Is Associated with Enhanced Epithelial-To-Mesenchymal Transition in Human Patient Breast Cancer Tissues and in Breast Cancer Cell Lines. *Cancers (Basel)* **11**, doi:10.3390/cancers11121967 (2019).
13 Stewart, M. K., Plante, I., Penuela, S. & Laird, D. W. Loss of Panx1 Impairs Mammary Gland Development at Lactation: Implications for Breast Tumorigenesis. *PLoS One* **11**, e0154162, doi:10.1371/journal.pone.0154162 (2016).
14 Sato, T., Neschadim, A., Lavie, A., Yanagisawa, T. & Medin, J. A. The engineered thymidylate kinase (TMPK)/AZT enzyme-prodrug axis offers efficient bystander cell killing for suicide gene therapy of cancer. *PLoS One* **8**, e78711, doi:10.1371/journal.pone.0078711 (2013).
15 Sun, Y.-Y., Zhang, T.-R., Liu, F.-F., Liu, H.-F. & Zhao, S.-d. Regulatory effect of the pannexin1 channel on invasion and migration of testicular cancer Tcam-2 cells and its possible mechanism. *Zhonghua Nan Ke Xue* **26**, 24-30 (2020).
16 Schalper, K. A., Carvajal-Hausdorf, D. & Oyarzo, M. P. Possible role of hemichannels in cancer. *Front Physiol* **5**, 237, doi:10.3389/fphys.2014.00237 (2014).
17 Xiang, X. *et al.* Pannexin 1 inhibits rhabdomyosarcoma progression through a mechanism independent of its canonical channel function. *Oncogenesis* **7**, 89-106 (2018).
18 O'Donnell, B. L. & Penuela, S. Skin in the game: pannexin channels in healthy and cancerous skin. *Biochemical Journal* **480**, 1929-1949, doi:10.1042/BCJ20230176 (2023).
19 O'Leary, N. A. *et al.* Reference sequence (RefSeq) database at NCBI: current status, taxonomic expansion, and functional annotation. *Nucleic Acids Res* **44**, D733-745, doi:10.1093/nar/gkv1189 (2016).
20 Ma, W., Hui, H., Pelegrin, P. & Surprenant, A. Pharmacological characterization of pannexin-1 currents expressed in mammalian cells. *Journal of Pharmacology and Experimental Therapeutics* **328**, 409-418 (2009).
21 Cunningham, F. *et al.* Ensembl 2022. *Nucleic Acids Res* **50**, D988-D995, doi:10.1093/nar/gkab1049 (2022).

22 Li, S., Tomic, M. & Stojilkovic, S. S. Characterization of novel Pannexin 1 isoforms from rat pituitary cells and their association with ATP-gated P2X channels. *Gen Comp Endocrinol* **174**, 202-210, doi:10.1016/j.ygcen.2011.08.019 (2011).
23 Baranova, A. *et al.* The mammalian pannexin family is homologous to the invertebrate innexin gap junction proteins. *Genomics* **83**, 706-716 (2004).
24 Turmel, P. *et al.* Characterization of pannexin1 and pannexin3 and their regulation by androgens in the male reproductive tract of the adult rat. *Mol Reprod Dev* **78**, 124-138, doi:10.1002/mrd.21280 (2011).
25 Abitbol, J. *et al.* Double deletion of Panx1 and Panx3 affects skin and bone but not hearing. *Journal of Molecular Medicine* **97**, 723-726, doi:10.1007/s00109-019-01779-9 (2019).
26 Sanchez-Pupo, R. E. *et al.* Pannexin 2 is expressed in murine skin and promotes UVB-induced apoptosis of keratinocytes. *Mol Biol Cell* **33**, 1-14, doi:10.1091/mbc.E21-08-0387) (2022).
27 Xiang, X. *et al.* Quercetin induces pannexin 1 expression via an alternative transcript with a translationally active 5' leader in rhabdomyosarcoma. *Oncogenesis* **11**, 9, doi:10.1038/s41389-022-00384-9 (2022).
28 Sriram, A., Bohlen, J. & Teleman, A. A. Translation acrobatics: how cancer cells exploit alternate modes of translational initiation. *EMBO Rep* **19**, doi:10.15252/embr.201845947 (2018).
29 Salat-Canela, C., Sesé, M., Peula, C., Ramón y Cajal, S. & Aasen, T. Internal translation of the connexin 43 transcript. *Cell Commun Signal* **12**, 31, doi:10.1186/1478-811X-12-31 (2014).
30 Smyth, J. W. & Shaw, R. M. Autoregulation of connexin43 gap junction formation by internally translated isoforms. *Cell Rep* **5**, 611-618, doi:10.1016/j.celrep.2013.10.009 (2013).
31 James, C. C., Zeitz, M. J., Calhoun, P. J., Lamouille, S. & Smyth, J. W. Altered translation initiation of Gja1 limits gap junction formation during epithelial-mesenchymal transition. *Mol Biol Cell* **29**, 797-808, doi:10.1091/mbc.E17-06-0406 (2018).
32 Salat-Canela, C., Sese, M., Peula, C., Ramon y Cajal, S. & Aasen, T. Internal translation of the connexin 43 transcript. *Cell Commun Signal* **12**, 31, doi:10.1186/1478-811X-12-31 (2014).
33 Basheer, W. A. *et al.* Stress response protein GJA1-20k promotes mitochondrial biogenesis, metabolic quiescence, and cardioprotection against ischemia/reperfusion injury. *JCI Insight* **3**, doi:10.1172/jci.insight.121900 (2018).
34 Basheer, W. A. *et al.* GJA1-20k Arranges Actin to Guide Cx43 Delivery to Cardiac Intercalated Discs. *Circ Res* **121**, 1069-1080, doi:10.1161/CIRCRESAHA.117.311955 (2017).
35 Kotini, M. *et al.* Gap junction protein Connexin-43 is a direct transcriptional regulator of N-cadherin in vivo. *Nat Commun* **9**, 3846, doi:10.1038/s41467-018-06368-x (2018).
36 Zeitz, M. J. *et al.* Dynamic UTR Usage Regulates Alternative Translation to Modulate Gap Junction Formation during Stress and Aging. *Cell Rep* **27**, 2737-2747 e2735, doi:10.1016/j.celrep.2019.04.114 (2019).
37 Palatinus, J. A. *et al.* GJA1-20k Rescues Cx43 Localization and Arrhythmias in Arrhythmogenic Cardiomyopathy. *Circ Res* **132**, 744-746, doi:10.1161/CIRCRESAHA.122.322294 (2023).

38 James, C. C. & Smyth, J. W. Alternative mechanisms of translation initiation: An emerging dynamic regulator of the proteome in health and disease. *Life Sci* **212**, 138-144, doi:10.1016/j.lfs.2018.09.054 (2018).
39 Kearse, M. G. & Wilusz, J. E. Non-AUG translation: a new start for protein synthesis in eukaryotes. *Genes Dev* **31**, 1717-1731, doi:10.1101/gad.305250.117 (2017).
40 Boassa, D. *et al.* Pannexin1 Channels Contain a Glycosylation Site That Targets the Hexamer to the Plasma Membrane. *J Biol Chem* **282**, doi:10.1074/jbc.M702422200 (2007).
41 Penuela, S. *et al.* Pannexin 1 and pannexin 3 are glycoproteins that exhibit many distinct characteristics from the connexin family of gap junction proteins. *J Cell Sci* **120**, 3772-3783, doi:10.1242/jcs.009514 (2007).
42 Kozak, M. Point mutations define a sequence flanking the AUG initiator codon that modulates translation by eukaryotic ribosomes. *Cell* **44**, 283-292, doi:10.1016/0092-8674(86)90762-2 (1986).
43 Sandilos, J. K. *et al.* Pannexin 1, an ATP release channel, is activated by caspase cleavage of its pore-associated C-terminal autoinhibitory region. *J Biol Chem* **287**, 11303-11311, doi:10.1074/jbc.M111.323378 (2012).
44 Chekeni, F. B. *et al.* Pannexin 1 channels mediate 'find–me' signal release and membrane permeability during apoptosis. *Nature* **467**, 863-867, doi:10.1038/nature09413 (2011).
45 Billaud, M. *et al.* A molecular signature in the pannexin1 intracellular loop confers channel activation by the a1 adrenoreceptor in smooth muscle cells. *Sci Signal* **8**, doi:10.1126/scisignal.2005824 (2015).
46 Weilinger, N. L. *et al.* Metabotropic NMDA receptor signaling couples Src family kinases to pannexin-1 during excitotoxicity. *Nat Neurosci* **19**, 432-442, doi:10.1038/nn.4236 (2016).
47 Weilinger, N. L., Tang, P. L. & Thompson, R. J. Anoxia-induced NMDA receptor activation opens pannexin channels via Src family kinases. *J Neurosci* **32**, 12579-12588, doi:10.1523/JNEUROSCI.1267-12.2012 (2012).
48 Consortium, F. *et al.* A promoter-level mammalian expression atlas. *Nature* **507**, 462-470, doi:10.1038/nature13182 (2014).
49 Kanamori-Katayama, M. *et al.* Unamplified cap analysis of gene expression on a single-molecule sequencer. *Genome Res* **21**, 1150-1159, doi:10.1101/gr.115469.110 (2011).
50 Lizio, M. *et al.* Gateways to the FANTOM5 promoter level mammalian expression atlas. *Genome Biol* **16**, 22, doi:10.1186/s13059-014-0560-6 (2015).
51 Weber, R. *et al.* Monitoring the 5'UTR landscape reveals isoform switches to drive translational efficiencies in cancer. *Oncogene* **42**, 638-650, doi:10.1038/s41388-022-02578-2 (2023).
52 Duvaud, S. *et al.* Expasy, the Swiss Bioinformatics Resource Portal, as designed by its users. *Nucleic Acids Res* **49**, W216-W227, doi:10.1093/nar/gkab225 (2021).
53 Duckert, P., Brunak, S. & Blom, N. Prediction of proprotein convertase cleavage sites. *Protein Eng Des Sel* **17**, 107-112, doi:10.1093/protein/gzh013 (2004).
54 Gupta, R. & Brunak, S. Prediction of glycosylation across the human proteome and the correlation to protein function. *Pac Symp Biocomput*, 310-322 (2002).

55 Nouri-Nejad, D. *et al.* Pannexin 1 mutation found in melanoma tumor reduces phosphorylation, glycosylation, and trafficking of the channel-forming protein. *Molecular Biology of the Cell* **32**, 376-390, doi:10.1091/mbc.E19-10-0585 (2021).
56 Wang, J., Mim, C., Dahll, G. & Barro-Soria, R. A metastasis-associated Pannexin1 mutant (Panx1$^{1-89}$) forms a minimalist ATP release channel. *bioRxiv*, doi:10.1101/2024.03.12.584732 (2024).
57 Vervoort, S. J. *et al.* Targeting transcription cycles in cancer. *Nat Rev Cancer* **22**, 5-24, doi:10.1038/s41568-021-00411-8 (2022).
58 Goldman, D. & Domschke, K. Making sense of deep sequencing. *Int J Neuropsychopharmacol* **17**, 1717-1725, doi:10.1017/S1461145714000789 (2014).
59 Boyce, A. K. J., Epp, A. L., Nagarajan, A. & Swayne, L. A. Transcriptional and post-translational regulation of pannexins. *Biochim Biophys Acta Biomembr* **1860**, 72-82, doi:10.1016/j.bbamem.2017.03.004 (2018).
60 Xiao, J. H., Davidson, I., Matthes, H., Garnier, J. M. & Chambon, P. Cloning, expression, and transcriptional properties of the human enhancer factor TEF-1. *Cell* **65**, 551-568, doi:10.1016/0092-8674(91)90088-g (1991).
61 Diaz de Arce, A. J., Noderer, W. L. & Wang, C. L. Complete motif analysis of sequence requirements for translation initiation at non-AUG start codons. *Nucleic Acids Res* **46**, 985-994, doi:10.1093/nar/gkx1114 (2018).
62 Touriol, C. *et al.* Generation of protein isoform diversity by alternative initiation of translation at non-AUG codons. *Biol Cell* **95**, 169-178, doi:10.1016/s0248-4900(03)00033-9 (2003).
63 Schuller, A. P., Wu, C. C., Dever, T. E., Buskirk, A. R. & Green, R. eIF5A Functions Globally in Translation Elongation and Termination. *Mol Cell* **66**, 194-205 e195, doi:10.1016/j.molcel.2017.03.003 (2017).
64 Sendoel, A. *et al.* Translation from unconventional 5' start sites drives tumour initiation. *Nature* **541**, 494-499, doi:10.1038/nature21036 (2017).
65 Peabody, D. S. Translation initiation at non-AUG triplets in mammalian cells. *J Biol Chem* **264**, 5031-5035 (1989).
66 Smith, L. M., Kelleher, N. L. & Consortium for Top Down, P. Proteoform: a single term describing protein complexity. *Nat Methods* **10**, 186-187, doi:10.1038/nmeth.2369 (2013).
67 Mou, L. *et al.* Structural basis for gating mechanism of Pannexin 1 channel. *Cell Res* **30**, 452-454, doi:10.1038/s41422-020-0313-x (2020).
68 Ruan, Z., Orozco, I. J., Du, J. & Lu, W. Structures of human pannexin 1 reveal ion pathways and mechanism of gating. *Nature* **584**, 646-651, doi:10.1038/s41586-020-2357-y (2020).
69 Kuzuya, M. *et al.* Structures of human pannexin-1 in nanodiscs reveal gating mediated by dynamic movement of the N terminus and phospholipids. *Sci Signal* **15**, eabg6941, doi:10.1126/scisignal.abg6941 (2022).
70 O'Donnell, B. L. *et al.* Pannexin 1 and Pannexin 3 differentially regulate the tumorigenic properties of cutaneous squamous cell carcinoma. *bioRxiv*, doi:10.1101/2024.04.08.588550 (2024).
71 Spagnol, G., Sorgen, P. L. & Spray, D. C. Structural order in Pannexin 1 cytoplasmic domains. *Channels (Austin)* **8**, 157-166, doi:10.4161/chan.28854 (2014).

72 Penuela, S., Bhalla, R., Nag, K. & Laird, D. Glycosylation Regulates Pannexin Intermixing and Cellular Localization. *Molecular Biology of the Cell* **20**, 4313–4323, doi:10.1091/mbc.e09-01-0067 (2009).
73 Sang, Q. *et al.* A pannexin 1 channelopathy causes human oocyte death. *Sci Transl Med* **11**, doi:10.1126/scitranslmed.aav8731 (2019).
74 Cruz-Munoz, W., Man, S., Xu, P. & Kerbel, R. S. Development of a preclinical model of spontaneous human melanoma central nervous system metastasis. *Cancer Res* **68**, 4500-4505, doi:10.1158/0008-5472.CAN-08-0041 (2008).
75 Williams, D. J., Puhl, H. L., 3rd & Ikeda, S. R. Rapid modification of proteins using a rapamycin-inducible tobacco etch virus protease system. *PLoS One* **4**, e7474, doi:10.1371/journal.pone.0007474 (2009).
76 Chiu, Y. H. *et al.* A quantized mechanism for activation of pannexin channels. *Nat Commun* **8**, 14324, doi:10.1038/ncomms14324 (2017).
77 Chiu, Y. H. *et al.* Deacetylation as a receptor-regulated direct activation switch for pannexin channels. *Nat Commun* **12**, 4482, doi:10.1038/s41467-021-24825-y (2021).
78 Aasi, S. *et al.* New onset of keratoacanthomas after vismodegib treatment for locally advanced basal cell carcinomas: a report of 2 cases. *JAMA Dermatol* **149**, 242-243, doi:10.1001/jamadermatol.2013.1798 (2013).
79 Kent, W. J. *et al.* The human genome browser at UCSC. *Genome Res* **12**, 996-1006, doi:10.1101/gr.229102 (2002).
80 UniProt, C. UniProt: the Universal Protein Knowledgebase in 2023. *Nucleic Acids Res* **51**, D523-D531, doi:10.1093/nar/gkac1052 (2023).
81 Hessa, T. *et al.* Molecular code for transmembrane-helix recognition by the Sec61 translocon. *Nature* **450**, 1026-1030, doi:10.1038/nature06387 (2007).
82 Tsirigos, K. D., Peters, C., Shu, N., Kall, L. & Elofsson, A. The TOPCONS web server for consensus prediction of membrane protein topology and signal peptides. *Nucleic Acids Res* **43**, W401-407, doi:10.1093/nar/gkv485 (2015).
83 Cserzö, M., Wallin, E., Simon, I., von Heijne, G. & Elofsson, A. Prediction of transmembrane alpha-helices in prokaryotic membrane proteins: the dense alignment surface method. *Protein Eng* **10**, 673-676, doi:10.1093/protein/10.6.673 (1997).
84 Hirokawa, T., Boon-Chieng, S. & Mitaku, S. SOSUI: classification and secondary structure prediction system for membrane proteins. *Bioinformatics* **14**, 378-379 (1998).
85 Hallgren, J. *et al.* DeepTMHMM predicts alpha and beta transmembrane proteins using deep neural networks. *bioRxiv*, doi:10.1101/2022.04.08.487609 (2022).
86 Pierleoni, A. *et al.* MemPype: a pipeline for the annotation of eukaryotic membrane proteins. *Nucleic Acids Res* **39**, W375-380, doi:10.1093/nar/gkr282 (2011).
87 Tran, N. H. *et al.* Deep learning enables de novo peptide sequencing from data-independent-acquisition mass spectrometry. *Nat Methods* **16**, 63-66, doi:10.1038/s41592-018-0260-3 (2019).
88 Tran, N. H., Zhang, X., Xin, L., Shan, B. & Li, M. De novo peptide sequencing by deep learning. *Proc Natl Acad Sci U S A* **114**, 8247-8252, doi:10.1073/pnas.1705691114 (2017).
89 Sun, W. *et al.* Glycopeptide database search and de novo sequencing with PEAKS GlycanFinder enable highly sensitive glycoproteomics. *Nat Commun* **14**, 4046, doi:10.1038/s41467-023-39699-5 (2023).

90 Omasits, U., Ahrens, C. H., Muller, S. & Wollscheid, B. Protter: interactive protein feature visualization and integration with experimental proteomic data. *Bioinformatics* **30**, 884-886, doi:10.1093/bioinformatics/btt607 (2014).

91 Schindelin, J. *et al.* Fiji: an open-source platform for biological-image analysis. *Nat Methods* **9**, 676-682, doi:10.1038/nmeth.2019 (2012).

92 Leighton, S. E. *et al.* Cx31.1 can selectively intermix with co-expressed connexins to facilitate its assembly into gap junctions. *Journal of Cell Science*, jcs.261631, doi:10.1242/jcs.261631 (2024).

Figure 1

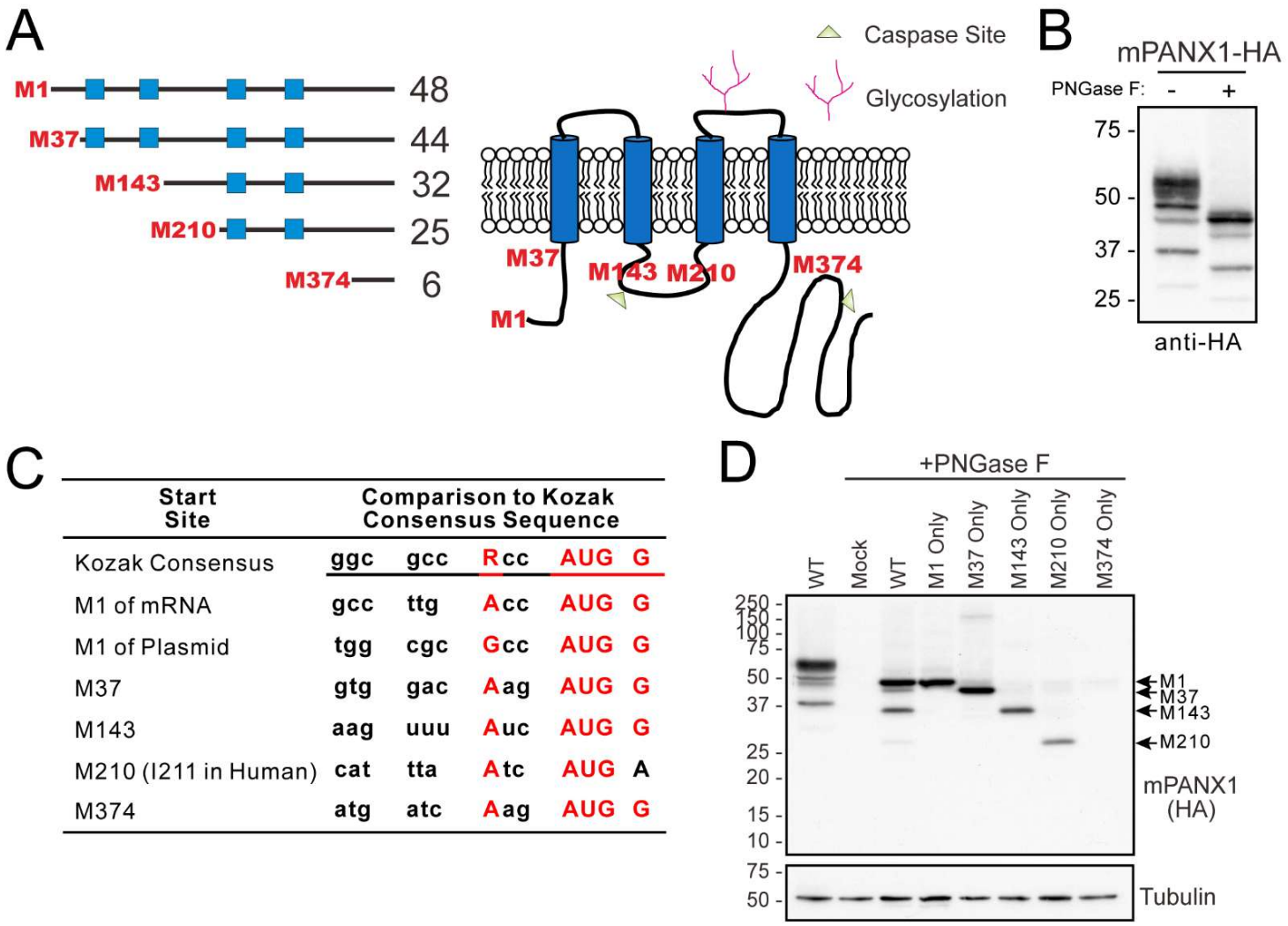

Start Site	Comparison to Kozak Consensus Sequence				
Kozak Consensus	ggc	gcc	Rcc	AUG	G
M1 of mRNA	gcc	ttg	Acc	AUG	G
M1 of Plasmid	tgg	cgc	Gcc	AUG	G
M37	gtg	gac	Aag	AUG	G
M143	aag	uuu	Auc	AUG	G
M210 (I211 in Human)	cat	tta	Atc	AUG	A
M374	atg	atc	Aag	AUG	G

Figure 2

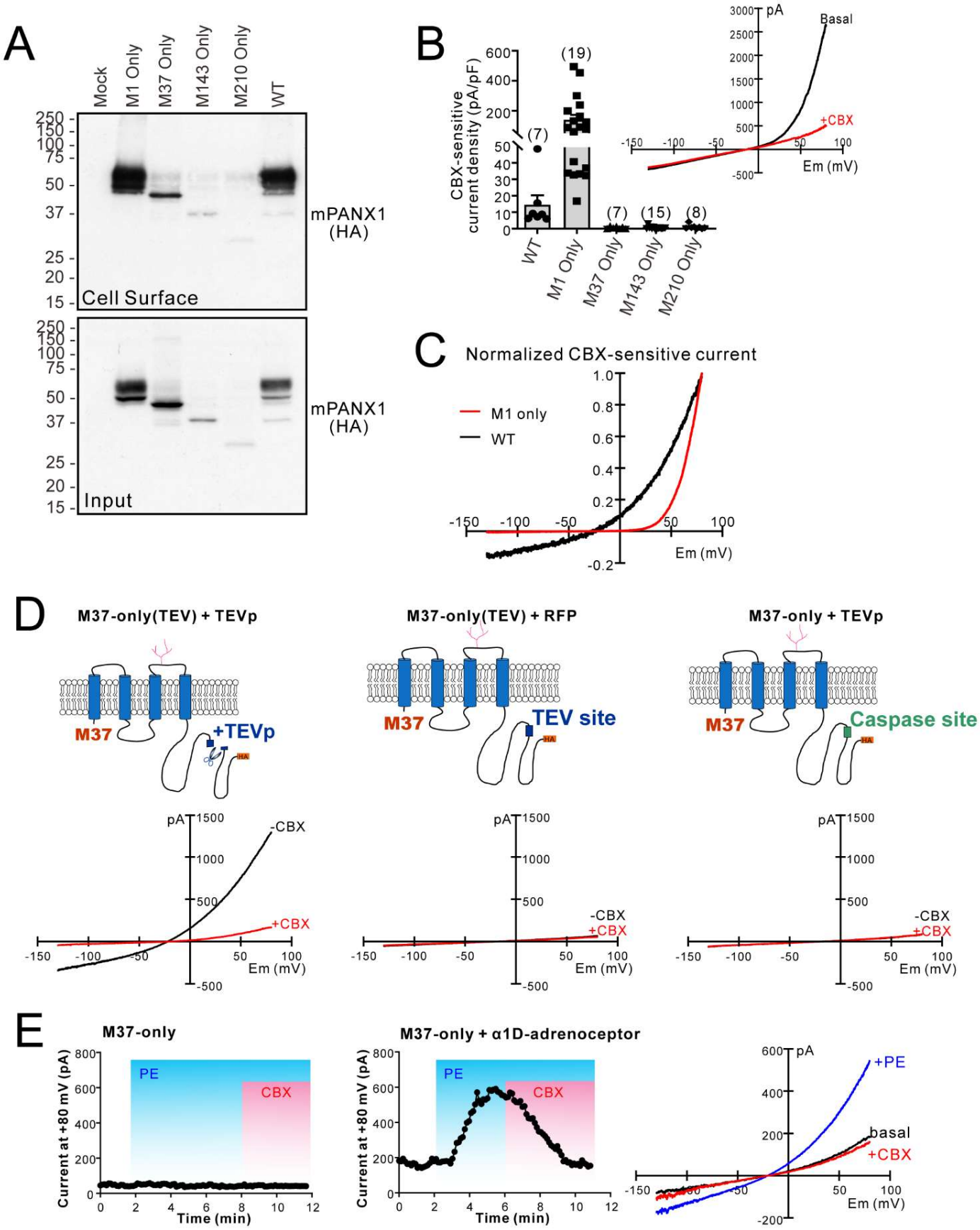
A
Mock
M1 Only
M37 Only
M143 Only
M210 Only
WT
mPANX1 (HA)
Cell Surface
Input
B
CBX-sensitive current density (pA/pF)
(19)
(7)
(7)
(15)
(8)
WT
M1 Only
M37 Only
M143 Only
M210 Only
pA
Basal
+CBX
Em (mV)
C
Normalized CBX-sensitive current
M1 only
WT
Em (mV)
D
M37-only(TEV) + TEVp
M37
+TEVp
M37-only(TEV) + RFP
M37
TEV site
M37-only + TEVp
M37
Caspase site
pA
-CBX
+CBX
Em (mV)
E
M37-only
M37-only + α1D-adrenoceptor
PE
CBX
Current at +80 mV (pA)
Time (min)
+PE
basal
+CBX
Em (mV)

Figure 3

A

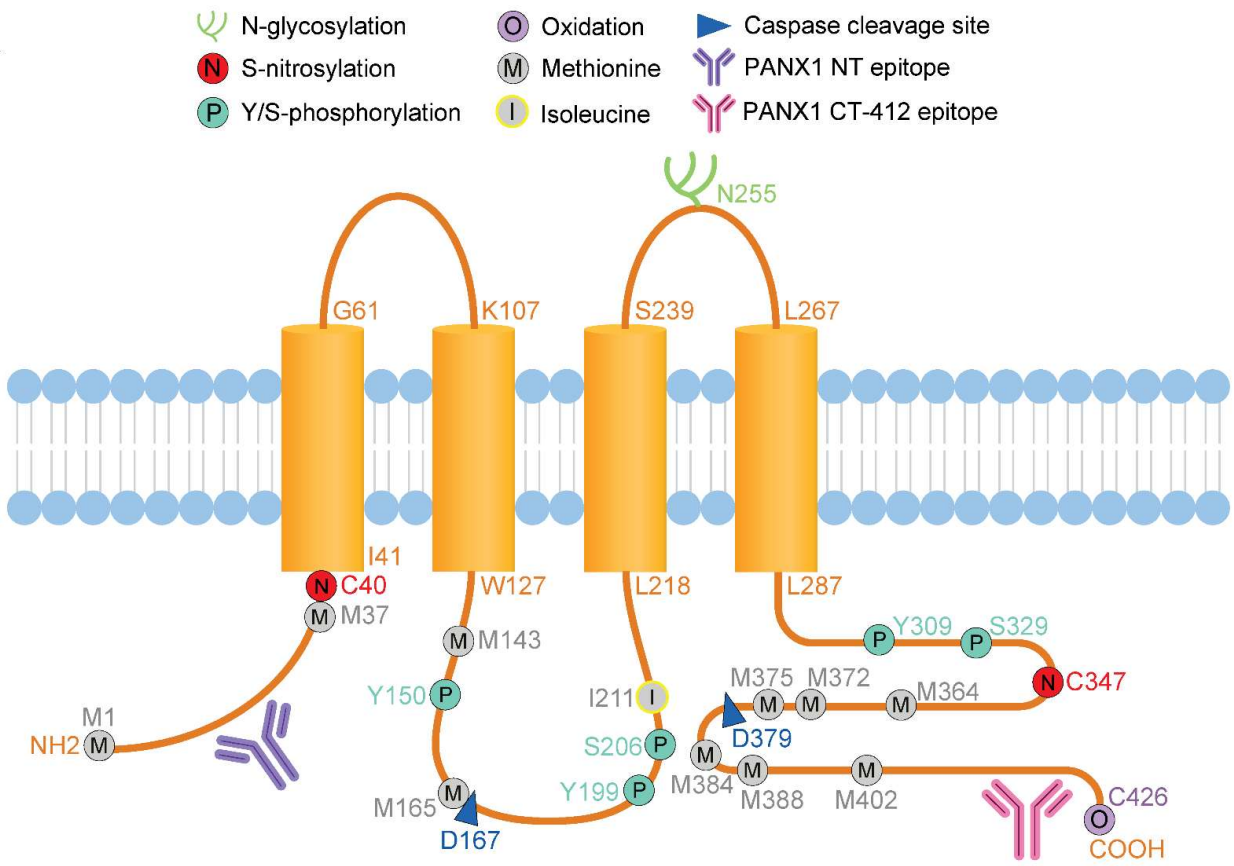

B

hPANX1 Topology from Potential Start Site	Length (aa)	Predicted MW (kDa)
M1 — TM1 TM2 TM3 TM4 — COOH	426	48.0
M37 — TM1 TM2 TM3 TM4 — COOH	390	44.0
M143 — TM3 TM4 — COOH	284	32.0
M165 — TM3 TM4 — COOH	262	29.5
I211 — TM3 TM4 — COOH	216	24.3
M364 — COOH	63	7.0
M372 — COOH	55	6.1
M375 — COOH	52	5.7
M384 — COOH	43	4.8
M388 — COOH	39	4.4
M402 — COOH	25	2.8

C

Start Site	Comparison to Kozak Consensus Sequence				
Kozak	gcc	gcc	Rcc	AUG	G
M1	gcc	gca	Gcc	AUG	G
M37	gug	gac	Aag	AUG	G
M143	aag	uuu	Auc	AUG	G
M165	gac	cuu	Gac	AUG	A
I211	aau	uua	Auc	AUC	A
M364	auc	gac	Cca	AUG	C
M372	aac	cuu	Ggc	AUG	A
M375	aug	auc	Aag	AUG	G
M384	aaa	acu	Ccc	AUG	U
M388	ucu	gca	Gag	AUG	A
M402	cuc	caa	Ggu	AUG	A

D

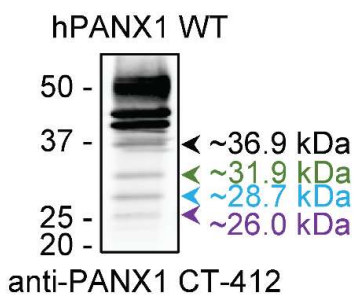

Figure 4

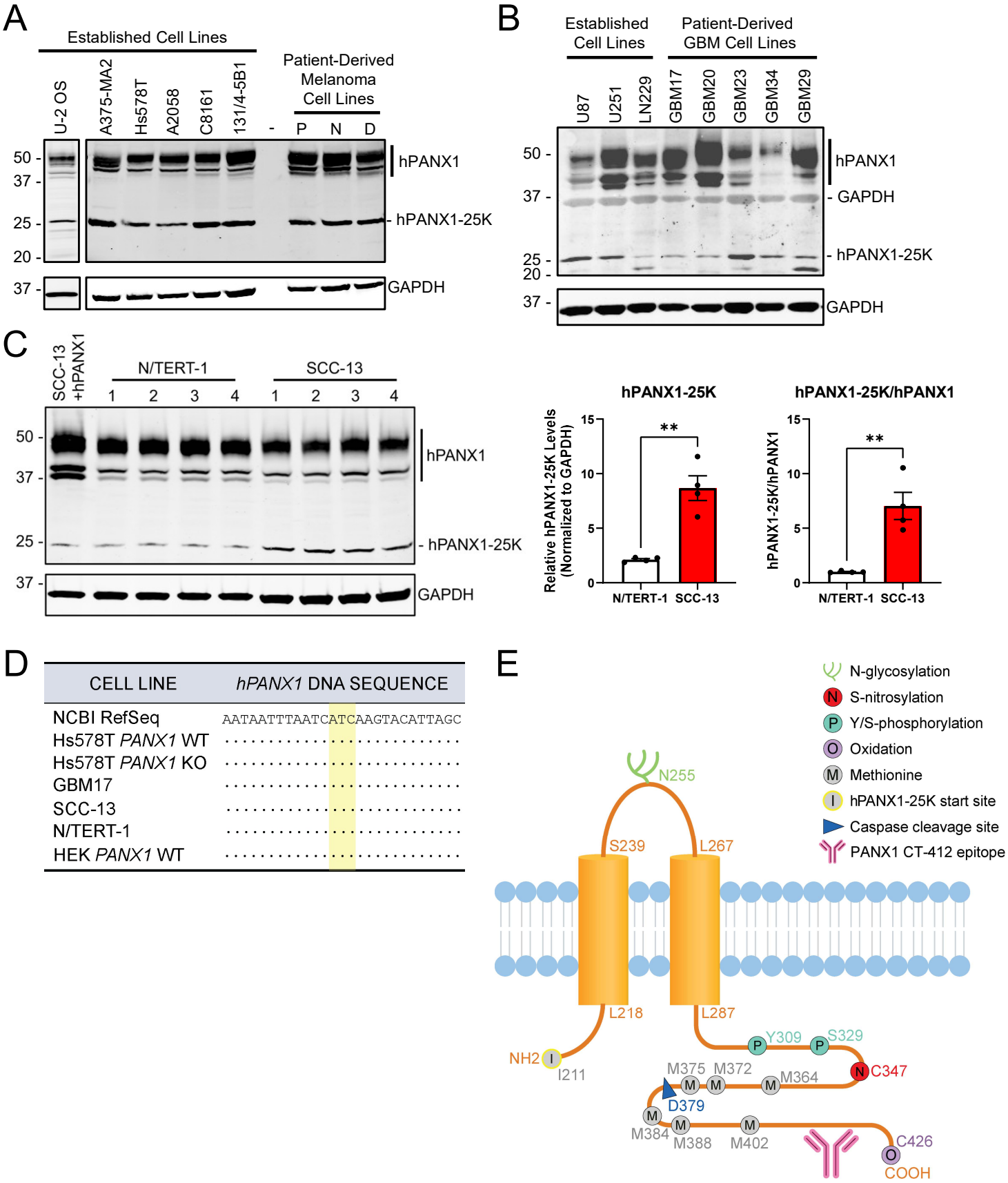
A
Established Cell Lines
U-2 OS
A375-MA2
Hs578T
A2058
C8161
131/4-5B1
Patient-Derived Melanoma Cell Lines
-
P
N
D
50
37
25
20
37
hPANX1
hPANX1-25K
GAPDH
B
Established Cell Lines
Patient-Derived GBM Cell Lines
U87
U251
LN229
GBM17
GBM20
GBM23
GBM34
GBM29
50
37
25
20
37
hPANX1
GAPDH
hPANX1-25K
GAPDH
C
SCC-13 +hPANX1
N/TERT-1
SCC-13
1
2
3
4
1
2
3
4
50
37
25
37
hPANX1
hPANX1-25K
GAPDH
hPANX1-25K
Relative hPANX1-25K Levels (Normalized to GAPDH)
15
10
5
0
**
N/TERT-1
SCC-13
hPANX1-25K/hPANX1
hPANX1-25K/hPANX1
15
10
5
0
**
N/TERT-1
SCC-13
D
CELL LINE
hPANX1 DNA SEQUENCE
NCBI RefSeq
AATAATTTAATCATCAAGTACATTAGC
Hs578T PANX1 WT
Hs578T PANX1 KO
GBM17
SCC-13
N/TERT-1
HEK PANX1 WT
E
N-glycosylation
S-nitrosylation
Y/S-phosphorylation
Oxidation
Methionine
hPANX1-25K start site
Caspase cleavage site
PANX1 CT-412 epitope
N255
S239
L267
L218
L287
NH2
I211
Y309
S329
M375
M372
M364
C347
D379
M384
M388
M402
C426
COOH

Figure 5

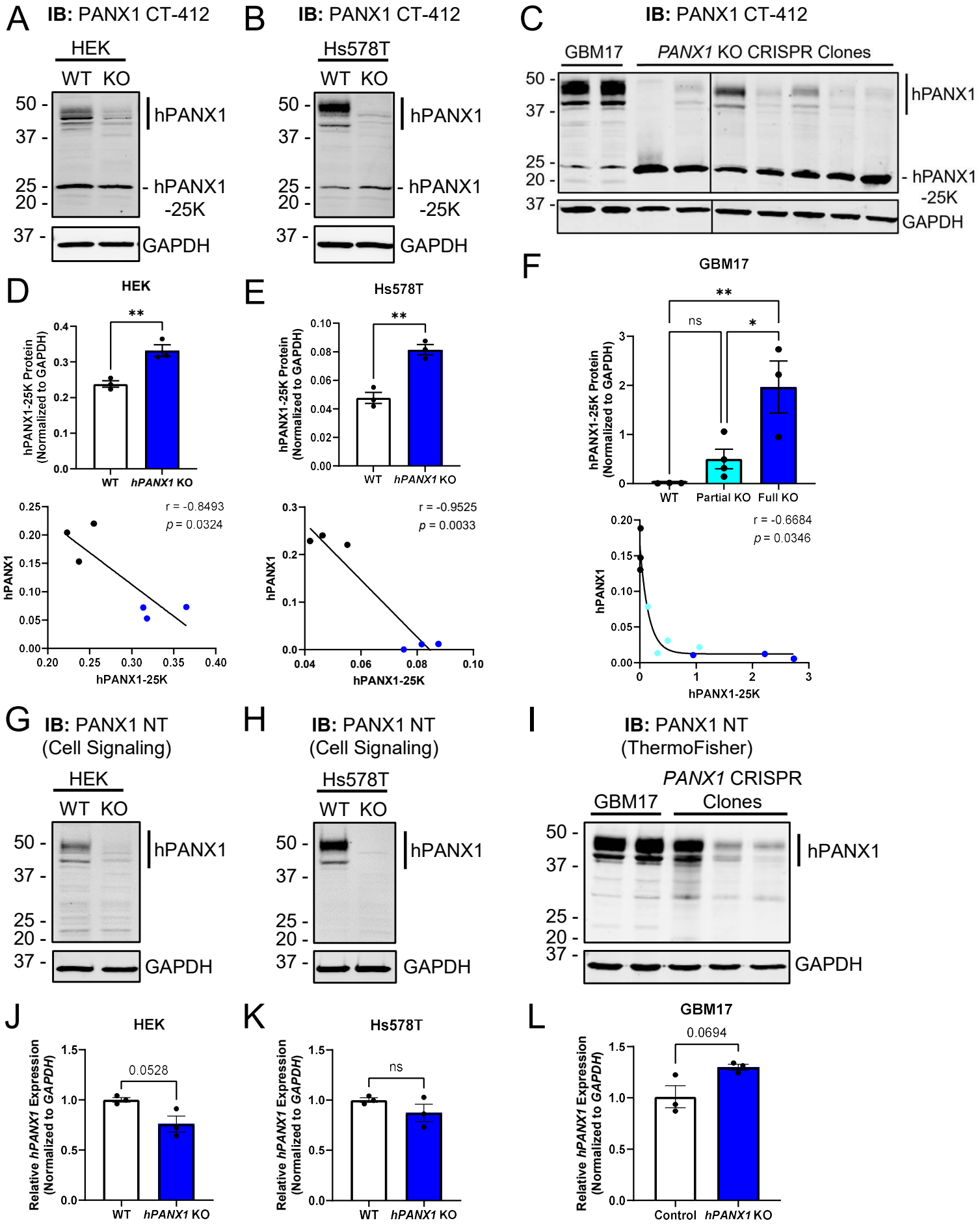
A
IB: PANX1 CT-412
HEK
WT KO
50 -
37 -
25 -
20 -
37 -
hPANX1
hPANX1 -25K
GAPDH
B
IB: PANX1 CT-412
Hs578T
WT KO
C
IB: PANX1 CT-412
GBM17
PANX1 KO CRISPR Clones
D
HEK
hPANX1-25K Protein (Normalized to GAPDH)
WT
hPANX1 KO
r = -0.8493
p = 0.0324
hPANX1
hPANX1-25K
E
Hs578T
r = -0.9525
p = 0.0033
F
GBM17
ns
Partial KO
Full KO
r = -0.6684
p = 0.0346
G
IB: PANX1 NT (Cell Signaling)
H
IB: PANX1 NT (Cell Signaling)
I
IB: PANX1 NT (ThermoFisher)
PANX1 CRISPR Clones
J
HEK
Relative hPANX1 Expression (Normalized to GAPDH)
0.0528
K
Hs578T
L
GBM17
0.0694
Control

Figure 6

A

IP: PANX1 CT-412
Stain: GelCode Blue

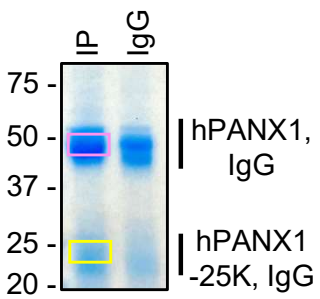

IP: PANX1 CT-412
IB: PANX1 CT-412

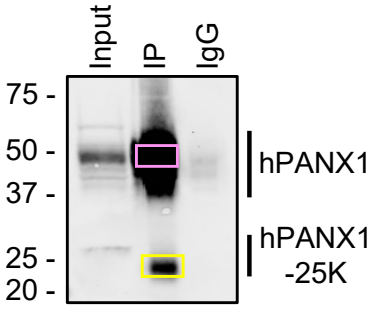

B

>sp|Q96RD7|PANX1_HUMAN Pannexin-1 OS=Homo sapiens OX=9606 GN=PANX1 PE=1 SV=4

```
  1 MAIAQLATEY VFSDFLLKEP TEPKFKGLRL ELAVDKMVTC IAVGLPLLLI SLAFAQEISI GTQISCFSPS SFSWRQAAFV
 81 DSYCWAAVQQ KNSLQSESGN LPLWLHKFFP YILLLFAILL YLPPLFWRFA AAPHICSDLK FIMEELDKVY NRAIKAAKSA
161 RDLDMRDGAC SVPGVTENLG QSLWEVSESH FKYPIVEQYL KTKKNSNNLI IKYISCRLLT LIIILLACIY LGYYFSLSSL
241 SDEFVCSIKS GILRNDSTVP DQFQCKLIAV GIFQLLSVIN LVVYVLLAPV VVYTLFVPFR QKTDVLKVYE ILPTFDVLHF
321 KSEGYNDSLL YNLFLEENIS EVKSYKCLKV LENIKSSGQG IDPMLLLTNL GMIKMDVVDG KTPMSAEMRE EQGNQTAELQ
401 GMNIDSETKA NNGEKNARQR LLDSSC
```

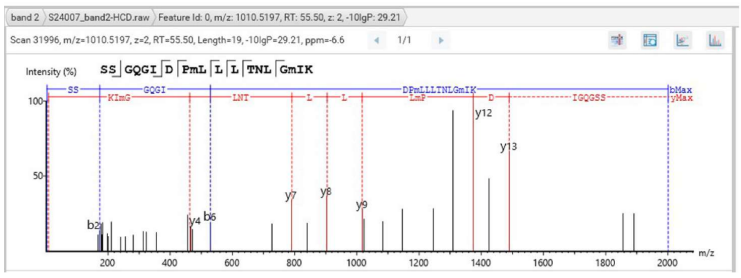

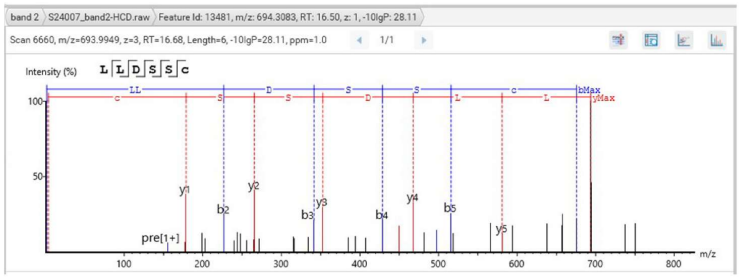

Figure 7

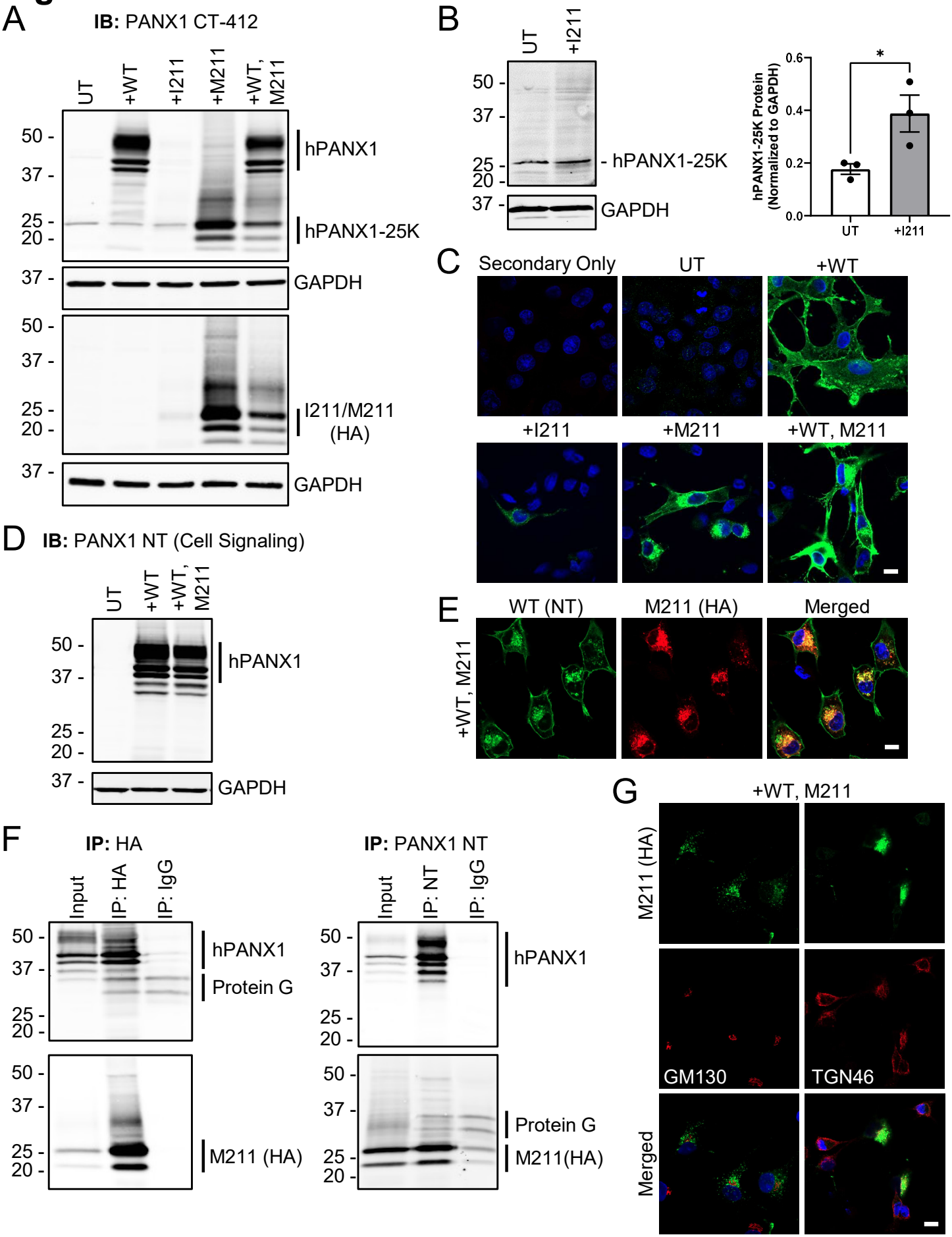
A
IB: PANX1 CT-412
UT
+WT
+I211
+M211
+WT, M211
50 -
37 -
25 -
20 -
hPANX1
hPANX1-25K
37 -
GAPDH
50 -
37 -
25 -
20 -
I211/M211 (HA)
37 -
GAPDH
B
UT
+I211
50 -
37 -
25 -
20 -
- hPANX1-25K
37 -
GAPDH
hPANX1-25K Protein (Normalized to GAPDH)
0.6
0.4
0.2
0.0
*
UT
+I211
C
Secondary Only
UT
+WT
+I211
+M211
+WT, M211
D
IB: PANX1 NT (Cell Signaling)
UT
+WT
+WT, M211
50 -
37 -
25 -
20 -
hPANX1
37 -
GAPDH
E
WT (NT)
M211 (HA)
Merged
+WT, M211
F
IP: HA
Input
IP: HA
IP: IgG
50 -
37 -
25 -
20 -
hPANX1
Protein G
50 -
37 -
25 -
20 -
M211 (HA)
IP: PANX1 NT
Input
IP: NT
IP: IgG
50 -
37 -
25 -
20 -
hPANX1
50 -
37 -
25 -
20 -
Protein G
M211(HA)
G
+WT, M211
M211 (HA)
GM130
TGN46
Merged

Figure 8

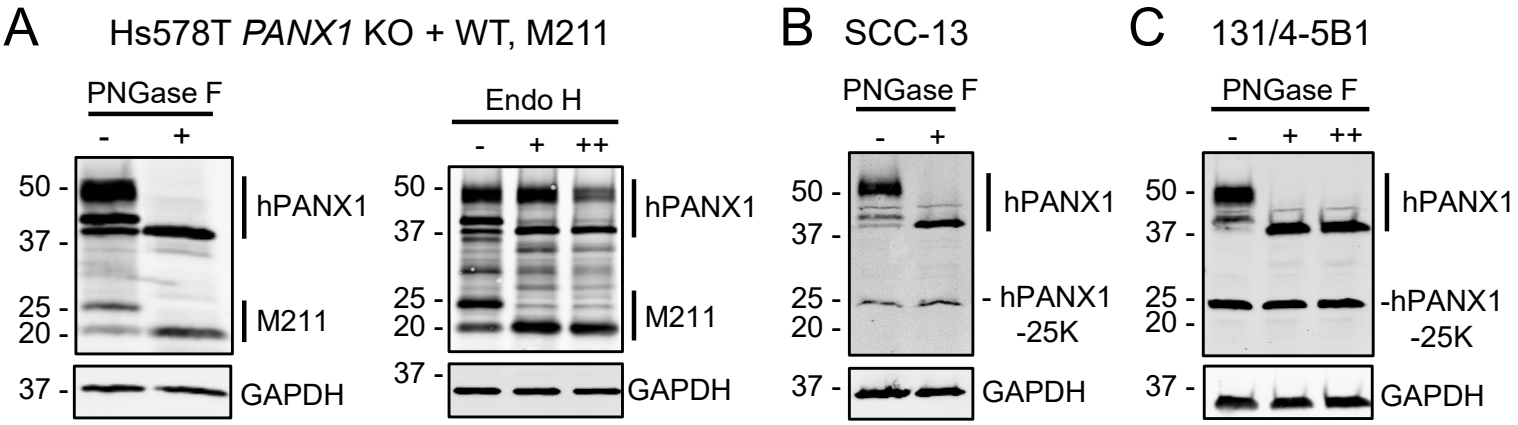

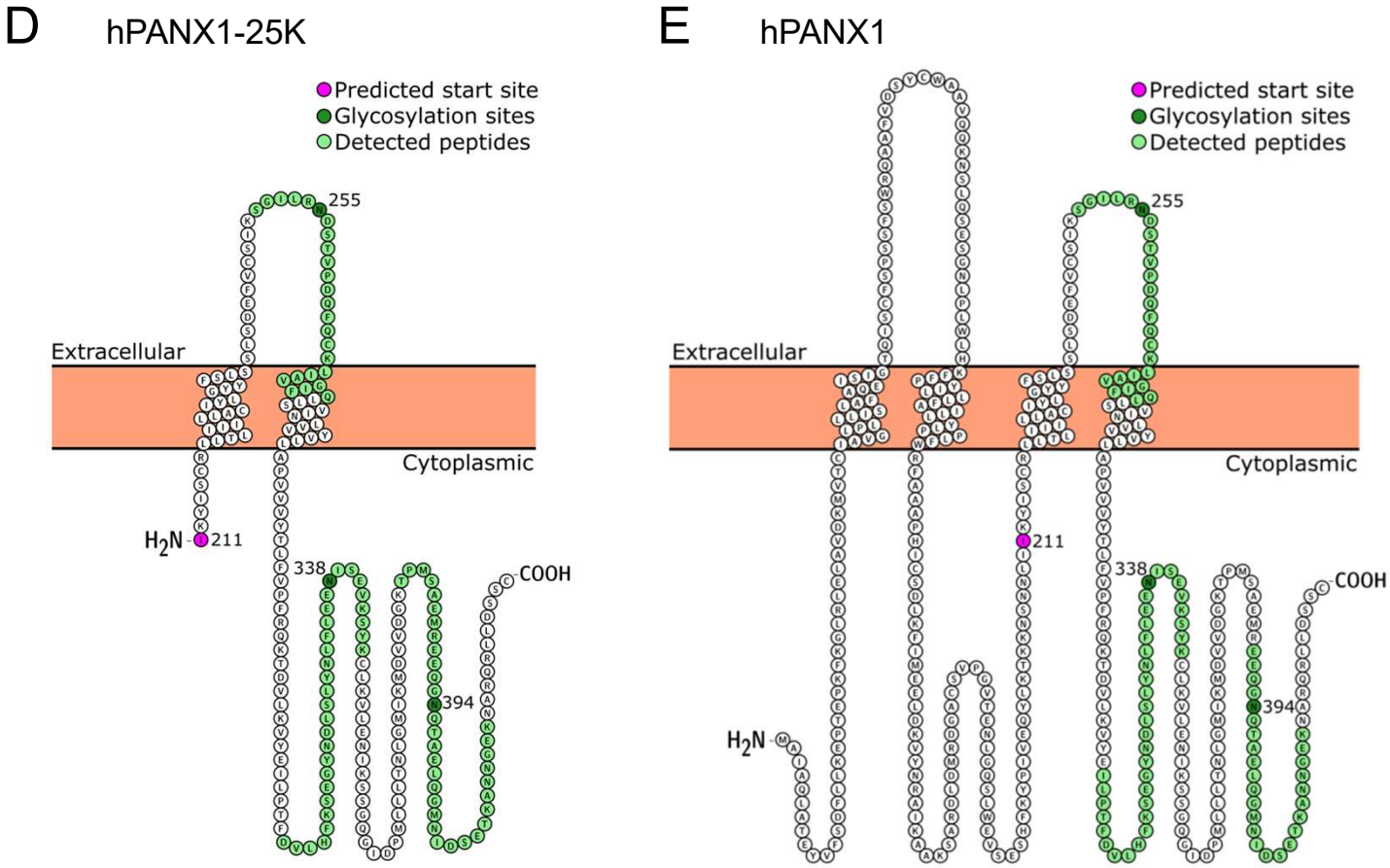

F

SeqName	Position	Potential*
PANX1_HUMAN 211-426	255, NDST	0.5484
PANX1_HUMAN 211-426	338, NISE	0.6411
PANX1_HUMAN 211-426	394, NQTA	0.5390

*Predicted N-glycosylation potential in hPANX1 211-426 sequence (NetNGlyc 1.0). Threshold=0.5

G

SeqName	Position	Potential*
sp_Q96RD7_PANX1_HUMAN	255, NDST	0.4663
sp_Q96RD7_PANX1_HUMAN	338, NISE	0.6030
sp_Q96RD7_PANX1_HUMAN	394, NQTA	0.5217

*Predicted N-glycosylation potential in hPANX1 1-426 sequence (NetNGlyc 1.0). Threshold=0.5

Figure 9

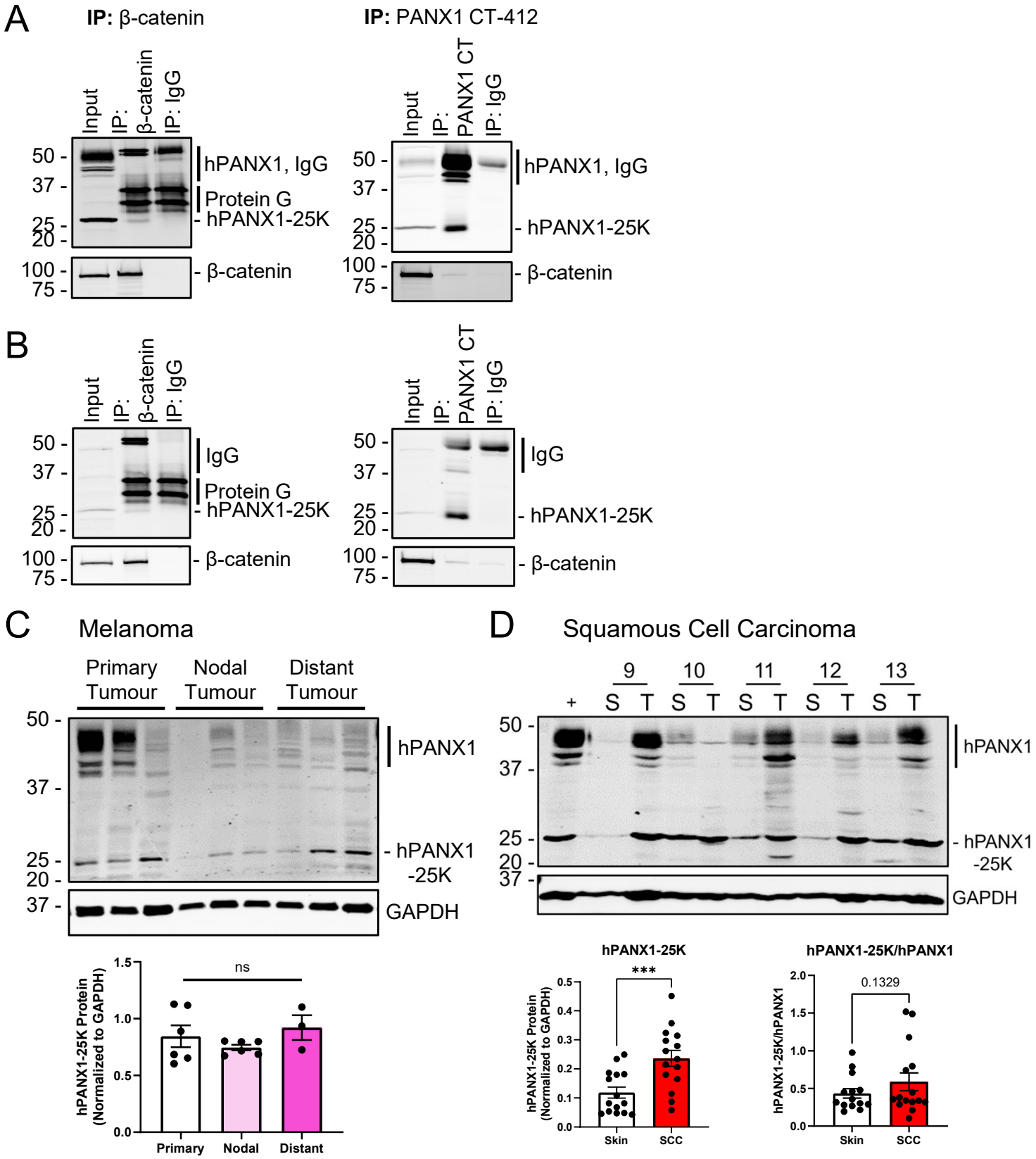
A
IP: β-catenin
IP: PANX1 CT-412
Input
IP: β-catenin
IP: IgG
Input
IP: PANX1 CT
IP: IgG
50 -
37 -
25 -
20 -
100 -
75 -
hPANX1, IgG
Protein G
- hPANX1-25K
- β-catenin
B
IgG
C
Melanoma
Primary Tumour
Nodal Tumour
Distant Tumour
hPANX1
- hPANX1 -25K
GAPDH
hPANX1-25K Protein (Normalized to GAPDH)
ns
Primary
Nodal
Distant
D
Squamous Cell Carcinoma
9
10
11
12
13
+
S
T
hPANX1-25K
***
Skin
SCC
hPANX1-25K/hPANX1
0.1329